NATIONAL ADVISORY COMMITTEE FOR AERONAUTICS

TECHNICAL NOTE 4035

IMPINGEMENT OF CLOUD DROPLETS ON 36.5-PERCENT-THICK

JOUKOWSKI AIRFOIL AT ZERO ANGLE OF ATTACK AND

DISCUSSION OF USE AS CLOUD MEASURING

INSTRUMENT IN DYE-TRACER TECHNIQUE

By R. J. Brun and Dorothea E. Vogt

Lewis Flight Propulsion Laboratory
Cleveland, Ohio

NACA

NATIONAL ADVISORY COMMITTEE FOR AERONAUTICS

TECHNICAL NOTE 4035

IMPINGEMENT OF CLOUD DROPLETS ON 36.5-PERCENT-THICK JOUKOWSKI AIRFOIL

AT ZERO ANGLE OF ATTACK AND DISCUSSION OF USE OF CLOUD MEASURING

INSTRUMENT IN DYE-TRACER TECHNIQUE

By R. J. Brun and Dorothea E. Vogt

SUMMARY

The trajectories of droplets in the air flowing past a 36.5-percent-thick Joukowski airfoil at zero angle of attack were determined. The amount of water in droplet form impinging on the airfoil, the area of droplet impingement, and the rate of droplet impingement per unit area on the airfoil surface were calculated from the trajectories and cover a large range of flight and atmospheric conditions. With the detailed impingement information available, the 36.5-percent-thick Joukowski airfoil can serve the dual purpose of use as the principal element in instruments for making measurements in clouds and of a basic shape for estimating impingement on a thick streamlined body.

Methods and examples are presented for illustrating some limitations when the airfoil is used as the principal element in the dye-tracer technique.

INTRODUCTION

A commonly used technique for making measurements in icing clouds, either in flight or in icing tunnels, involves the collection of ice on cylinders of different diameters exposed to the airstream. This technique is known as the rotating multicylinder method and is described in reference 1. Another technique for measuring cloud droplet sizes principally in tunnels and with temperatures above freezing is described in reference 2 as the dye-tracer technique. In this method, a blotter-wrapped body, such as a cylinder or airfoil for which theoretical droplet impingement data are available, is exposed to an airstream containing a dyed-water spray cloud. The amount and local distribution of dye residue in the blotter are analyzed and are compared with theoretical values in order to obtain the sizes of the droplets in the impinging cloud.

Several other methods involving photography, sampling techniques, light scattering, droplet impaction, or combinations of two or more of these principles, such as are described in reference 3 (see also references listed in ref. 3), have been employed in the process of developing cloud measuring instruments. The scope of this report is confined to presenting data and discussion intended to refine the use of the dye-tracer technique.

The impingement data obtained from droplet trajectory calculations are required for either the rotating multicylinder method or the dye-tracer technique. The calculation of droplet trajectories requires a knowledge of the airflow field surrounding the aerodynamic body being studied. In order that the trajectory calculations apply in principle, the calculated air velocity components surrounding the body must be the same as those existing in the atmosphere during the measurements. The velocity components used in the calculations are usually obtained from the solution of theoretically derived flow equations for a body immersed in an ideal incompressible fluid. The equations do not account for viscosity, separation of the flow from the body, effects of compressibility, turbulence, and other factors. The effects of compressibility of the air on droplet trajectories have been found to be negligible up to the flight critical Mach number of the body (ref. 1). With most well designed aerodynamic bodies and when used for measuring atmospheric cloud droplets of interest in icing, the effect of viscosity is small as it is confined to the boundary-layer region.

A concern for the effect of flow separation around cylinders is expressed in reference 2, in which a comparison of the theoretical and wind tunnel experimental surface velocities on cylinders is given. The comparison is repeated herein as figure 1. It is apparent that the ratios of local surface velocity to free-stream velocity differ over the entire cylinder surface. The difference between experiment and theory may be due to early separation of the flow. This separation may induce a flow pattern ahead of the cylinder that is not attendant to a right circular cylinder but rather to some virtual shape related to the position of separation on the cylinder surface. The large differences in the local velocity on the cylinder surface indicate that the airflow field ahead of the cylinder may be considerably different from the theoretical flow field. Consequently, actual droplet trajectories may be different from the theoretical calculations of reference 1 and may contribute to errors and to such anomalies as discrepancies in the cloud measurements (droplet-size distribution and liquid-water content) when the size of the cylinder is varied. These discrepancies are related to cylinder size in such a manner as to be inconsistent with the theoretical analyses of reference 1. The varied deviations of measured surface velocity among different-sized cylinders from the theoretical surface velocity (fig. 1) imply an explanation for the cylinder-size trend.

The experimental work of reference 2 suggests the use of a blunt-nosed body such as the cylinder but with a streamlined trailing section that minimizes flow separation. The blunt-nosed shapes are preferred, especially when used with the dye-tracer technique described in reference 2. The principal reasons for this preference are that the limits of impingement and distribution of water on the surface are more easily measured on bluff bodies.

On the basis of wind tunnel experience, a thick Joukowski airfoil section was investigated as a possible streamlined, blunt-nosed body. A Joukowski airfoil has many of the desirable geometric qualities and, in addition, is amenable to simple calculations of the flow field. A 60-percent-thick Jouskowski airfoil section was tested in the wind tunnel and was found to have serious airflow separation. A section arbitrarily reduced to a thickness of 36.5 percent was a satisfactory bluff body with only a small difference between the theoretical and experimental surface velocities (fig. 2). This airfoil gives a surface velocity ratio within 4 percent of the calculated ideal. When the air velocity distribution on the 36.5-percent-thick airfoil was found satisfactory and the airfoil retained the desired bluntness, no other airfoil was examined.

Droplet trajectories were calculated for the 36.5-percent-thick Joukowski airfoil at the NACA Lewis laboratory. The calculations help explain some of the difficulties, which are discussed later, encountered in the use of cylinders. With detailed information on droplet impingement available, the 36.5-percent-thick Joukowski airfoil serves a dual purpose. Besides providing an aerodynamic body for replacing cylinders when they exhibit undesirable surface velocity distributions in cloud measuring instruments, the calculations serve as an immediate contribution of information on impingement on very thick airfoil sections used in some applications such as radar housings. Streamlined struts closely resembling thick-sectioned Joukowski airfoils are also often used for mounting instruments, fuel tanks, and armament projecting into the airstream.

CALCULATIONS OF DROPLET TRAJECTORIES

In order to find the rate and distribution of droplet impingement on the surface of a body, it is necessary to determine the cloud-droplet trajectories with respect to the body. The method used for the 36.5-percent-thick Joukowski airfoil in calculating the droplet trajectories is essentially the same as described in reference 1 for the cylinder. Assumptions necessary for the solution of the problem are: (1) At a large distance ahead of the body the droplets are at rest with respect to the air; (2) the only external force acting on the droplets, as the airfoil approaches the droplets, is the drag force due to the relative velocity of the air with respect to the droplets; and (3) the droplets are always spherical and do not change in size.

Differential Equations of Droplet Motion

The differential equations that describe the motion of the droplets are obtained by equating the drag force with the rate of change of momentum of the droplet. The equations apply to the motion of droplets in a plane coincident with the airfoil section as shown in figure 3. The airfoil location in the coordinate system used in other NACA reports (such as ref. 4) is retained herein. The geometric chord line of the airfoil is collinear with the x-axis of the rectangular coordinate system, and the leading edge is placed at the origin of the coordinates. At an infinite distance ahead of the airfoil, the uniform airflow carrying the cloud droplets is assumed to be approaching the airfoil from the negative x-direction and parallel to the x-axis.

The equations of motion, as derived in reference 1, are

$$\left. \begin{array}{l} \dfrac{dv_x}{d\tau} = \dfrac{C_D Re}{24} \dfrac{1}{K} (u_x - v_x) \\[3mm] \dfrac{dv_y}{d\tau} = \dfrac{C_D Re}{24} \dfrac{1}{K} (u_y - v_y) \end{array} \right\} \tag{1}$$

where Re is the local Reynolds number with respect to the droplet diameter $2a$ and the local relative velocity between the air and the droplet. (All symbols are defined in appendix A.) Thus,

$$Re = \frac{2a\rho_a V}{\mu} \sqrt{(u_x - v_x)^2 + (u_y - v_y)^2} \tag{2}$$

The coefficient in equation (2) is called the free-stream Reynolds number Re_0. Hence,

$$Re_0 \equiv \frac{2a\rho_a V}{\mu} \tag{3}$$

The dimensionless number K, the inertia parameter, is defined as

$$K \equiv \frac{\rho_w a^2 V}{\mu L} \tag{4}$$

The coefficient of drag C_D is obtained from experimental data as a function of the local droplet Reynolds number Re (ref. 5).

The equations are expressed in dimensionless form in order to maintain the number of calculations at a minimum and to simplify the presentation of the results. The dimensionless coordinates x and y are ratios of the actual distance to the chord length L, which is the unit of

length. The dimensionless air velocity components u_x and u_y and the droplet velocity components v_x and v_y are ratios of the actual velocity to the free-stream velocity, which is the unit of velocity. Time is expressed in terms of the dimensionless quantity $\tau = tV/L$. The unit of time is the time required to go a distance L at a speed V.

An examination of equations (1) and (2) shows that the characteristics of the trajectories depend only on the values of the two dimensionless parameters K and Re_0. Thus, a unique droplet trajectory exists for each combination of K and Re_0.

Method of Solution

The differential equations of motion (eqs. (1)) are difficult to solve because values of the velocity components and the factor containing the coefficient of drag depend on the position and velocity of the droplet at each instant and, therefore, are not known until the trajectory is traced. The values of these quantities must be fed into the equations as a trajectory is developed. This was accomplished by using a mechanical differential analyzer constructed at the NACA Lewis laboratory for this purpose (ref. 6). The results were obtained in the form of plots of droplet trajectories in the coordinates of figure 3.

The velocity field around the airfoil, required for the solution of the trajectory equations, was obtained from equations for incompressible, ideal flow around a Joukowski airfoil such as given in reference 7. A simple translation of coordinates and scale is necessary when the usual equations for the Joukowski airfoil (ref. 7) are used in order to place the airfoil as shown in figure 4 with one chord as the unit of length. The surface coordinate points are presented in table I, and the airfoil shape is illustrated in figure 4. The relation between chordwise and surfacewise positions, which is often very useful, is given in figure 5.

The equations of motion were solved for various values of the parameter K. The inertia parameter K is a measure of the droplet size, the flight speed and size of the airfoil, and the viscosity of the air through the relation

$$K = 1.704 \times 10^{-12} \, d^2 U / \mu L \tag{5}$$

The density of water, 1.94 slugs per cubic foot, is included in the constant. For each value of K, a series of trajectories was computed for each of several values of free-stream Reynolds number

$$Re_0 = 4.813 \times 10^{-6} \, d\rho_a U / \mu \tag{6}$$

A convenient graphical means for determining values of the dimensionless parameters K and Re_0 in terms of airplane speed (free-stream velocity), chord length, altitude, and droplet size is presented in appendix B of reference 4.

A dimensionless parameter φ defined as

$$\varphi \equiv \frac{Re_0^2}{K} = 13.594 \frac{\rho_a^2 L U}{\mu} \tag{7}$$

is also used in presenting the data. The parameter φ is valuable in that it is not a function of droplet size. The parameter φ is an important concept in the interpretation of cloud measurements in which the droplet size is not measured directly and is an unknown that must be calculated (see ref. 1). The use of any two of the three dimensionless parameters K, Re_0, or φ will completely define a data point with respect to the flight and meteorological conditions.

IMPINGEMENT RESULTS

For a symmetrical airfoil at zero angle of attack, the airflow field for negative values of the y-ordinate is a mirror image of the flow field around the upper airfoil surface. Thus, only the impingement on the upper surface is presented.

The rate of water impingement and the manner in which it is distributed on the surface of the airfoil can be obtained if the starting point of a droplet trajectory is known with respect to the point of impingement on the surface. The starting ordinate y_0 at infinity of any impinging trajectory can be found in figure 6 with respect to the point of impingement on the surface. The values for the starting and ending positions of the trajectories are shown in figure 6 for five values of free-stream Reynolds number. For each value of Re_0, curves for several values of K are given. Since the curves for very low values of K are difficult to read from the scale used in presenting figure 6, the same data are plotted in figure 7 for three low values of K.

The calculated points for the curves are shown in figures 6 and 7 in order to give an appreciation of the precision of the curves. Information on precision is often necessary when the airfoil is used as the principal element of an instrument. Because the mechanical analogue used for the calculations is substantially a graphical method of solution, the data points in figure 6 have a tolerance of ± 0.001 on both values of s and values of y_0. In figure 7 the tolerance is ± 0.0005 for s and ± 0.0002 for y_0. The difference in tolerances is caused by the change in scale factors during the calculations. The tolerance for the values of

s · along the dashed line in figure 6 (s_{max}, described in following section) is ±0.002 because the determination of the point of tangency provided an added factor of uncertainty.

Extent of Impingement

The limit of impingement is determined by the point of tangency on the airfoil surface of the tangent trajectory. In figure 6 the limits of impingement s_{max} lie on the dashed lines, which are the loci of the termini of the curves and which determine the point of impingement of the tangent trajectory for each combination of K and Re_0. For convenience, the rearward limits are replotted in figure 8 as a function of K for various values of Re_0. The distances are measured on the airfoil surface from the point of intersection of the geometric chord line with the leading edge (fig. 3) in terms of the chord length. When the airfoil is used as the principal element of an instrument, the values of s_{max} as a function of K for various values of φ are often more useful. This is shown in figure 9.

Rate of Total Water Interception

The rate of total water interception, in pounds per hour per foot of wing span, is determined by the spacing of the tangent trajectories (fig. 3), by the speed of the aircraft, and by the liquid-water content in the cloud. The flight speed and size of the airfoil, as well as the droplet size in the cloud, are the principal variables that affect the spacing between the upper- and lower-surface tangent trajectories. For a symmetrical airfoil at zero angle of attack, the water that strikes the airfoil is divided equally between the top and bottom halves and, therefore, is proportional to twice the spacing between the x-axis and the ordinate $y_{0,tan}$ at infinity of the upper surface tangent trajectory. In figure 6, the values of $y_{0,tan}$ and those for s_{max} lie on the dashed lines. The rate of total water interception per unit span of the airfoil on that portion of the airfoil surface bounded by the upper and lower tangent trajectories can be calculated from the relation

$$W_{max} = 0.66 U w L y_{0,tan} \tag{8}$$

The rate of total water interception per unit of span can also be obtained from the collection efficiency E, which is defined as the ratio of the water contained in the droplets intercepted by the airfoil to the total water in the volume swept out of its path by the airfoil. On the basis of collection efficiency $E = y_{0,tan}/0.182$,

$$W_{max} = 0.12 U w L E \tag{9}$$

The values of E are given in figure 10 as a function of K for various values of Re_0. Again, because of the usefulness in the application, the collection efficiency is repeated in figure 11 for various values of φ.

Rate of Local Droplet Impingement

The local impingement rate on the airfoil surface is often desirable knowledge in the design of thermal anti-icing systems or when the airfoil is used as a principal element of an instrument. The rate of water impinging between any two given points on the airfoil surface may be found by applying the results of figures 6 and 7 in the relation

$$W = 0.33 U w L (y_{0,1} - y_{0,2}) \tag{10}$$

The local rate of droplet impingement per unit area of airfoil surface can be determined from the expression

$$W_\beta = 0.33 U w \frac{dy_0}{ds} = 0.33 U w \beta \tag{11}$$

The values of the local impingement efficiency β as a function of the airfoil distance s are given in figures 12 and 13. These values were obtained from the slopes of the curves in figures 6 and 7, respectively.

The values of β given in figures 12 and 13 are estimated to be in error by less than ± 1 percent. Since the rate of total water impinging is directly related to the area under the β curves, a check on computational accuracy of the values of β in figures 12 and 13 was also obtained by comparing the area under each β curve with values of collection efficiency in figure 10. The area values checked within ± 0.3 percent of the corresponding values for the rate of total water interception.

DISCUSSION OF RESULTS

Comparison of Impingement on 36.5- with 15-Percent-Thick

Joukowski Airfoils and Cylinder

A comparison of available data on collection efficiency and limit of impingement for three bodies that vary in thickness ratio is helpful when interpolation as a function of thickness ratio is necessary. Data for a 15-percent-thick Joukowski airfoil are presented in reference 8 and for the cylinder in reference 1. The cylinder is included for comparison because it can be considered as a symmetrical airfoil with a thickness ratio of 100 percent.

The collection efficiency for the 36.5-percent-thick Joukowski airfoil is presented in figures 10 and 11 in terms of K, Re_0, and φ. Langmuir has suggested the use of a modified K parameter (refs. 5 and 9). The advantage of this modified parameter is that the data in terms of K and Re_0 or φ are essentially reduced to a single curve. For any given set of operating and meteorological conditions, which are represented by one value of the modified parameter, the impingement characteristics of several bodies of different shape can be easily compared.

The modified K parameter is known as the K_0 parameter (see ref. 9) which is defined as

$$K_0 = K \frac{\lambda}{\lambda_s}$$

where λ is the range a droplet would have when projected into still air if the drag is based on experimentally determined values (also known as true range), and λ_s is the range of a droplet obeying Stokes' law of air drag for a sphere. The total collection efficiency E is given as a function of K_0 in figure 14 for 15- and 36.5-percent-thick Joukowski airfoils and a cylinder. The values of E as functions of K_0 are shown in figure 14 as a single-valued curve for each body. Although no proof of the significance of K_0 is available at this time, careful calculations reduce a family of curves, such as collection efficiency as a function of K and Re_0 shown in figure 10, to a very narrow band of curves which essentially can be presented as a single-valued curve for purposes of comparison. For any value of K_0, which represents the same operating and meteorological conditions for all three bodies, the collection efficiency decreases with increase in thickness ratio.

A comparison of the limit of impingement s_{max} is shown in figure 15. The extent decreases with decrease in thickness ratio except for low values of K_0. Low values of K_0 represent conditions of small droplets combined with large chord lengths and low speed. As an example for orientation, a value of K_0 of 0.078 could represent an altitude of 10,000 feet, a chord length of 18 inches, a speed of 200 miles per hour, and a droplet diameter of 18 microns.

Impingement in Clouds of Nonuniform Droplet Size

The data presented in figures 6 to 13 apply directly only to flights in clouds composed of droplets that are all uniform in size. The droplets in a cloud, however, may have a range of sizes. The design of equipment for protection against ice formation can be in error when based on a single droplet size such as the volume-median if a distribution of droplet

sizes is present in the cloud. The limit of impingement on the surface
is governed principally by the large droplets. Also, the total rate of
impingement can vary considerably with changes in the size distribution
of the cloud even though the liquid-water content and volume-median diam-
eter are maintained. When the airfoil section is used as an element of
a measuring instrument, the data in figures 6 to 13 must always be applied
in a modified (weighted) manner. The method of weighting the data is
discussed in detail in reference 2 in the application of cylinder data to
the dye-tracer technique and is reviewed briefly, along with the dye-
tracer technique, in appendix B herein.

USE OF AIRFOIL AS SENSING ELEMENT

An evaluation of the 36.5-percent-thick Joukowski airfoil as a sensing
element in an instrument can be made with illustrating examples. Much of
the discussion on the airfoil also applies to other geometric shapes, par-
ticularly cylinders, except that the range of limits of K and Re_0 may
vary.

Basic Requirements of a Sensing Element

A necessary requirement for a sensing element is that the unknown
being measured by the element must have a well defined variation with
respect to a known independent quantity. For example, the droplet size,
which is the unknown being measured by the Joukowski element, must be a
well defined function of either surface extent or collection rate (either
total or local, depending on which is used), which presumably is obtained
by measurement. For example, according to the curves in figures 9 and
11, a well defined function exists between the limit of impingement (fig.
9) or collection efficiency (fig. 11) and the inertia parameter K, which
contains the factor of droplet size, for values of K from 0.04 to 5.
Flight and meteorological conditions represented by values of K smaller
and larger than the limits stated reduce the sensitivity of the thick
Joukowski airfoil as a sensing element. Unfortunately, values of K less
than 0.04 are often encountered in icing tunnel and flight operations.
For example, for operation at 200 miles per hour, an altitude of 10,000
feet, and an airfoil chord length of 18 inches, K is less than 0.04 when
droplet diameters are less than about 8 microns. The upper limit, that
is, K greater than 5, represents droplets greater than 87 microns provided
the other conditions do not change.

The preceding example illustrates the desirability of using several
airfoils with different chord lengths (see ref. 10, appendix B) in measur-
ing clouds with wide distributions in droplet size. A change in airfoil
chord length has a large effect on the limits of sensitivity because the
chord length L appears in the expression for the inertia parameter K

as well as in the determination of other factors such as surface extent. If a 6-inch airfoil had been used in the preceding example, the values of K would have been three times larger (values of Re_0 are not affected by chord length), and the readings for either surface distance of impingement (figs. 8 and 9) or collection efficiency (figs. 10 and 11) would have been shifted into a region more favorable for the smallest droplets. This shift, however, hampers the large droplet measurements for which large airfoils are required.

Sensitivity for Droplet-Size Discrimination

In the dye-tracer technique and other methods, the determination of the droplet-size distribution requires a known correlation between droplet size and limit of impingement. For sensitivity, a measurable variation between droplet size and impingement limit is required. An appreciation for the sensitivity, as well as the judgment required in the selection of size of cloud measuring elements and their application, can be obtained from the following example. The following table presents a spectrum of droplet sizes and the corresponding values of parameters and dimensions that apply:

[Flight speed, 200 mph; altitude, 10,000 ft;
airfoil chord length, 18 in.]

Droplet diameter, d, microns	Inertia parameter, K	Free-stream Reynolds number, Re_0	Surface distance of impingement, s		
			Ratio to chord length	In.	In inches for droplet diameter difference of 2 microns
50	1.64	251	0.230	4.15	} 0.07
48	1.51	240	.227	4.08	
40	1.05	201	.206	3.71	} .09
38	.95	190	.201	3.62	
30	.59	150	.175	3.15	} .14
28	.52	140	.167	3.01	
20	.26	100	.128	2.30	} .23
18	.21	90	.115	2.07	
10	.066	50	.050	.90	.32
8	.042	40	.032	.58	.17
6	.024	30	.023	.41	[a].05
4	.010	20	.020	.36	[a].04
2	.003	10	.018	.32	

[a]Obtained from extrapolated curves in fig. 8.

The extent of impingement is given in the fourth column as a ratio of the actual distance to the chord length (obtained from fig. 8) and in

the fifth column in inches for an airfoil with an 18-inch chord. The
last column gives the difference in limit in inches for a 2-micron differ-
ence in diameter of the droplets. In the table the largest difference in
the limits and, therefore, the largest sensitivity, occurs between 10-
and 8-micron droplets although good sensitivity exists from 8- to 25-
micron diameters.

In the discussion of the dye-tracer technique presented in reference
2, 1/8-inch segments of blotter are used in the colorimetric analysis.
Thus, the sensitivity is limited to variations that take place on incre-
ments larger than 1/8 inch. In the example cited in the preceding table,
6-micron droplets cannot be differentiated from 4-micron droplets, and
38-micron droplets cannot be differentiated from 40-micron droplets when
1/8-inch segments are used. A size spectrum would be most accurate between
38 and 6 microns. If 1/16-inch segments are used (see ref. 10), some im-
provement is realized in the lower size range of the spectrum, but the
lower limit is not extended appreciably. As can be seen from the preced-
ing table, if the surface graduations were 1/16 inch apart, the lower
range sensitivity would be extended to include the 5-micron droplets.
This extention would be an improvement of 1 micron in diameter. However,
the use of 1/16-inch segments, especially near the stagnation line, im-
proves the accuracy in determining the local rate of water distribution
(W_β curve described in appendix B).

The limit of accuracy and sensitivity in the size spectrum (e.g.,
38- to 6-micron range in preceding example) will change when operating
and meteorological conditions change. As discussed in the preceding sec-
tion, a change in airfoil chord length has a large effect on the limits
of sensitivity. The small airfoils have a desired advantage in measuring
small droplets; however, decreasing the airfoil size introduces other
difficulties. Decreasing the chord length from 18 to 6 inches decreases
the surface distance (scale) on which the measurements are made, with a
consequent requirement of greater care and more sensitivity.

The preceding principles, actions, and conclusions apply equally well
to cylinders and other geometric shapes. It should be noted that a cylin-
der has different limits of sensitivity than an airfoil. Also, there are
differences in sensitivity among airfoils of varying thickness ratio and
shape as well as chord length mentioned in the preceding paragraph.

Masking effect of large droplets. - In the determination of droplet-
size distribution and liquid-water content, the masking effect of large
droplets is a source of error inherent with most instruments that depend
on impingement and retention of the cloud substance such as dye or ice
accretion. With these instruments the final measurement, for example,
the local rate of impingement on the surface of the element or total
collection efficiency, is a composite of contributions by droplets of
different sizes. The contribution from large drops may overwhelm the

contribution from the small droplets even though a large percentage of the total water in the cloud may be carried by the small droplets, because of the low collection efficiency of small droplets. This masking effect is illustrated with examples in appendix C obtained from table II.

In appendix C two widely differing droplet-size distributions (flights 1 and 3, table II) measured with an aeroscope (ref. 3) are taken as the standards with which comparisons are made. These distributions are applied to a 36.5-percent-thick Joukowski airfoil section used in such a manner that the local collection rate on chordwise sections of the airfoil surface is the principal measurable quantity. This method is used in the dye-tracer technique described in reference 2 and reviewed in appendix B herein. The droplet-size distributions are divided into size groups. The water contained in each size group (fractional part of total, as measured with aeroscope) is given in rows D and K for flights 1 and 3, respectively.

The example evaluations for flight 1 are made at five chordwise positions on the airfoil surface (approximately 1 in. apart (rows E to I)) in order to present a condensed table of calculations. (The curve for the local rate of water impingement as a function of surface distance (see appendix B) is established by a large number of analyses of punched segments (refs. 2 and 10). For flight 3 the evaluations are made at the stagnation line only.

Row E is an analysis at the airfoil stagnation line (s = 0) for flight 1. The rate of local droplet impingement β obtained from figures 12 and 13 is given along with the rate of water impingement on the airfoil contributed by each size group (product of β and water contained in each size group (row D)). The sum of the rates of water impingement contributed by each size group is the weighted local impingement efficiency. This value of weighted local impingement efficiency is 0.5482 at the stagnation line for flight 1. When the weighted value of β is used in equation (11), the local rate of water impingement W_β is obtained. This value is used for the W_β curve in the dye-tracer technique for determining the droplet-size distribution in the cloud (see appendix B).

Errors in the measurement of dye concentration in each punched segment will change the W_β curve used in determining the droplet-size distribution in a proportional manner. A change in the W_β curve can affect the reported droplet-size distribution appreciably among the small droplets. Because the error in measuring dye concentration shrinks the W_β ordinate and not the surface extent of impingement and because the droplet-size distribution obtained by the dye-tracer technique is a cumulative composite of contributions by different sizes starting with the largest size, the small droplets contributing a small fraction of the total dye can be indiscernible in the analysis. For example, an error of -5 percent in measuring the dye concentration lowers the W_β by 5 percent. Through

equation (11) the lowering of W_β can be considered in terms of a weighted local impingement efficiency β lowered by 5 percent. At the stagnation line in the example given in appendix C for flight 1 (row E), 5 percent lowers the value of weighted β by 0.0274. All the water impinging on the blotter at the stagnation line can be accounted for in the droplets between diameters of 57.5 and 12.6 microns. The amount of dye lost by the error is the same as that which is contributed by the 0- to 12.6-micron-diameter droplets. As can be seen by the analyses made in rows F to I, other positions on the airfoil surface do not aid in discerning these small droplets. When the droplets below 12.5 microns are indiscernible, the liquid-water content is only 0.89 as large as that measured by the aeroscope.

The analysis along the stagnation line for flight 3 (row L) shows that a 5-percent error obliterates the droplets between 0 and 7.5 microns. Elimination of these droplets makes the liquid-water content 0.95 as large as that measured with the aeroscope.

A safeguard against losing too many of the small droplet groups is provided in reference 10 by using an aspirator to determine liquid-water content and, also, to establish the local rate of water impingement curve (appendix B) at the airfoil stagnation line. Furthermore, the use of several airfoils of different sizes (ref. 10) improves the inherent sensitivity on local rates of impingement as was shown for limits of impingement.

Cylinder Surface Velocities

The problem of discrepancies in cloud measurements when the size of the cylinder was varied is mentioned in the INTRODUCTION. According to the trajectory calculations in reference 1 based on the classical theory of airflow around a right circular cylinder, final cloud measurements (droplet-size distribution and liquid-water content) should not be dependent on the size of the cylinder used. The cylinder-size trend experienced in the work reported in reference 2, in which the final results were dependent on the particular cylinder diameter used, is caused by factors other than the sensitivity discussed in the preceding sections. Furthermore, the trend is not part of the concept presented in reference 1 in which a group of cylinders of different sizes can be used for making cloud measurements.

Because of the different surface to free-stream velocity ratio measured on different-sized cylinders in the icing wind tunnel (fig. 1), it was suggested in reference 2 that the differences in cloud measurements obtained by different sizes of cylinders were due to differences in the flow fields surrounding the cylinders. If the point of view is taken that the difference in surface velocities between the 6- and 2-inch

cylinders (fig. 1) is caused by the degree of separation of flow from the
cylinder surface (fig. 16) and consequently by the location on the sur-
face of the two cylinders where separation begins, the difference in im-
pingement among the cylinders can be explained in part on the basis of
differences in the flow field. When flow separation occurs, the airflow
ahead of the cylinder is not that attendant to a cylinder but rather to
some virtual shape such as shown in figure 16 by the forward part of the
cylinder and the dashed lines. Since the trajectories of droplets are
governed by the environmental airflow pattern, the impingement is related
to the virtual shape caused by the flow separation.

Icing tunnel experiments beyond those reported in reference 2 have
shown that size trends were nearly eliminated when the cylinders were
replaced by 36.5-percent-thick Joukowski airfoils of different sizes.
The elimination of the size trend was due to the elimination of flow
separation as can be surmised from the surface velocity distribution
shown in figure 2.

The differences in curves of surface velocity shown in figure 1 for
different-sized cylinders may not apply under all operating conditions.
A safe procedure in the use of cylinders is to survey the surface velocity
on the cylinders with pressure taps. In order for a reasonable assurance
that the theoretical trajectory results of reference 1 apply, the velocity
survey should not reveal flow separation such as is revealed in figure 1.
A pressure tap survey of surface velocities with the cylinders mounted on
an airplane was made in flight in order to determine whether the separa-
tion deduced from figure 1 was largely affected by tunnel conditions such
as tunnel turbulence. In order to minimize end effects, both the 6- and
2-inch flight cylinders were 15 inches long, and the holes for the pres-
sure taps were located midway between the ends.

The flight results are shown in figure 17 with the theoretical and
6-inch cylinder curves of figure 1 taken in the icing tunnel. The flight
results are very comparable to the tunnel results in that the velocities
of the 2-inch cylinder are lower than for the larger cylinder in both
cases, and all are lower than the theoretical. The flight surface veloci-
ties on the 4.5-inch cylinder of the multicylinder set detailed in figure
16 of reference 1 are also shown in figure 17. Although the maximum ve-
locity measured on the 4.5-inch cylinder is slightly higher than on either
the 6- or 2-inch cylinder, the velocity everywhere is considerably lower
than the theoretical and, thus, lower than the values necessary for safe
application of the theoretical computations of reference 1. The somewhat
higher maximum velocities obtained on the 4.5-inch cylinder mounted as
part of the multicylinder set are not readily explainable. However, the
fact that this cylinder was only about 3 inches long as compared to 15
inches for the 6- and 2-inch-diameter cylinders and that the mounting was
slightly different may have a bearing on an explanation. The 4.5-inch
multicylinder was mounted as part of the multicylinder set.

Because the flight and tunnel velocity distributions on the surface of the cylinders are similar, the droplet impingement on the flight cylinders can be expected to behave in a manner similar to that on the tunnel cylinders.

CONCLUDING REMARKS

Viscosity was one of the effects mentioned in the INTRODUCTION that are not accounted for in theoretically derived flow fields. Although at present there is no direct experimental evidence evaluating the effect of viscosity on trajectories, there are reasons to believe that with most well designed aerodynamic bodies the effect of viscosity is small. An analytical evaluation of viscosity presented in reference 11 supports this point of view for the range of Reynolds numbers usually encountered in making natural cloud measurements from aircraft. Perhaps a simplified physical explanation of the reason the effect of viscosity on droplet trajectories around cylinders is negligible may be parallel to the explanation on why compressibility has small effect. The velocity field about the cylinder is influenced only near the cylinder surface by either compressibility or viscosity. Reference 1 shows for compressibility that when the flow field is affected only near the body, the effect is small on trajectories of droplets.

The replacement of cylinders by a Joukowski airfoil for measuring instruments is required only when the airflow around the cylinder is not comparable to the theoretical flow used in the calculations of reference 1. The 36.5-percent-thick Joukowski airfoil retains many of the desirable properties of the cylinder and has the necessary flow field that permits the application of calculated results in a range of operating conditions not possible with cylinders. The least desirable feature of the airfoil is that the shape changes as ice accumulates on the surface. This feature is of no consequence when the airfoil is used with the dye-tracer technique in tunnels.

As mentioned in the INTRODUCTION, the impingement data presented herein are also useful in estimating impingement on thick streamlined struts. Thick-sectioned struts that are over 15 percent thick probably do not differ from Joukouski airfoil sections in any manner that affects the collection efficiency appreciably when compared to a Joukowski airfoil section of the same thickness ratio. The surface extent of impingement is more sensitive than collection efficiency to details of shape (ref. 10). As demonstrated in reference 12, if a part of an airfoil section (such as the leading-edge region or forward 25-percent region, etc.) has the same shape and pressure distribution as its counterpart on another airfoil, the impingement on the two parts will be the same even though the other portions of the airfoil sections differ in both shape and pressure

distribution. On thick-sectioned bodies the distribution is concentrated on the leading edge, which eases the problem of estimating the surface impingement.

Lewis Flight Propulsion Laboratory
    National Advisory Committee for Aeronautics
        Cleveland, Ohio, July 9, 1957

APPENDIX A

SYMBOLS

a   droplet radius, ft (3.048×10^5 microns)

C_D coefficient of drag, dimensionless

d   droplet diameter, microns (3.28×10^{-6} ft)

E   collection efficiency, dimensionless

K   inertia parameter, $1.704 \times 10^{-12} \dfrac{d^2 U}{\mu L}$, dimensionless (density of water, 1.94 slugs/cu ft, included in constant)

K_0 modified inertia parameter, $\dfrac{\lambda}{\lambda_s} K$, dimensionless

L   airfoil chord length, ft

Re   local Reynolds number with respect to droplet, dimensionless

Re_0 free-stream Reynolds number with respect to droplet, $4.813 \times 10^{-6} \dfrac{d \rho_a U}{\mu}$, dimensionless

s   distance on surface of airfoil measured from leading-edge chord point, ratio to chord length

t   time, sec

U   flight speed, mph

u   local air velocity, ratio to free-stream velocity

V   free-stream velocity, ft/sec

v   local droplet velocity, ratio to free-stream velocity

W   rate of water impingement per unit span of airfoil, lb/(hr)(ft span)

W_β local rate of water impingement, lb/(hr)(sq ft)

w   liquid-water content in cloud, g/cu m

x,y   rectangular coordinates, ratio to chord length

β local impingement efficiency, $\dfrac{dy_0}{ds}$, dimensionless

θ central angle of cylinder measured from leading edge stagnation point, deg

λ true range of droplet as a projectile injected into still air, ft

λ_s range of droplet as a projectile following Stokes' law, ft

μ viscosity of air, slugs/(ft)(sec)

ρ density, slugs/cu ft

τ dimensionless time functions, $\tau = tV/L$

$$\varphi \equiv \frac{Re_0^2}{K} \equiv \frac{18\rho_a^2 LV}{\mu\rho_w}, \text{ dimensionless}$$

Subscripts:

a   air

l lower airfoil surface

max   maximum or total rate

s   airfoil surface

tan   tangent trajectory

u   upper airfoil surface

w   water

x,y   component coordinate direction

β local rate

0   free stream

APPENDIX B

REVIEW OF DYE-TRACER TECHNIQUE

The method is reviewed herein to present the background necessary for evaluating the use of the 36.5-percent-thick Joukowski airfoil as a sensing element in a cloud droplet instrument. The dye-tracer technique was developed in order to measure the droplet-size distribution and liquid-water content in a cloud. A blotter-wrapped body, such as a cylinder or the Joukowski airfoil studied herein, is exposed to an airstream containing a dyed-water spray cloud. In this technique, water treated with small quantities of water-soluble dye is injected in the form of droplets into the airstream ahead of the body by means of spray nozzles. At the point of impact and droplet absorption by the blotter, a permanent dye deposit is obtained. The amount of dye deposit on the blotter is directly proportional to the water impingement rate. The amount of dye trace obtained in a measured time interval can be determined by colorimetric analysis and converted into the quantity of water which produced it because the composition of the treated water is known. The local rate of water impingement W_β, total rate of water interception W_{max}, and the surface extent of impingement s_{max} are obtained from the colorimetric analysis.

The principal information obtained from the colorimetric analysis is the local rate of water impingement W_β as a function of surface distance s. Typical values of W_β are shown in figure 18 as the solid-line curve. The area under the curve is a measure of the total water impingement on the blotter. The area under the W_β curve is a composite of areas contributed by an unknown number of different droplet sizes in the cloud-size distribution. The object is to determine the cloud-size distribution from the shape of the solid-line curve in figure 18. The determination is made with the use of the calculated β curves (local impingement efficiency) shown in figures 12 and 13.

For simplicity in the presentation of the principles involved, the abscissa in figure 18 (airfoil surface distance of impingement) is arbitrarily divided into six equal increments. As is described in reference 2, the number and size of increments are usually governed by the size of the segments punched from the blotter for use in the colorimetric analysis (see fig. 12, ref. 2). The limit of impingement s_{max} is established by the largest droplets present in the droplet-size distribution. The actual diameter can be obtained from the values of s_{max} and impingement limit data presented in figures 8 and 9. The contribution of these largest droplets to the total area under the solid line is obtained by superposing in figure 18 the proper β curve (local rate of droplet impingement) obtained from figures 12 and 13. This superposition properly weighted for a fractional part of total water is shown in figure 18 as the dashed line

labeled 1. If the solid-line curve were a result of impingement by a
cloud composed of droplets uniform in size, curve 1 would coincide with
the solid curve. However, figure 18 indicates that the largest droplets
in the cloud contribute only the area under curve 1.

The next step is to determine the contribution by a smaller size
group. This group is assumed to have a limit of impingement at s_2.
Again, from the value of s_2 and the data of figures 8, 9, 12, and 13,
the area contribution by group 2 is found to be the area between the
dashed lines labeled 2 and 1. The procedure is repeated for s_3, and so
forth. Detailed procedure with working charts is given in reference 2.

APPENDIX C

EVALUATION OF MASKING EFFECT

An evaluation of the errors that actually are involved in the masking effect can be made with a realistic cloud distribution. The cloud data used in the following evaluation were obtained in flights through atmospheric clouds and are reported in reference 3. The measurements were made with an oil-stream photomicrographic aeroscope in which the cloud droplets were continuously captured in a stream of oil and photographed by a photomicrographic camera.

The basic data used in table II (number of droplets in each size group) are obtained from the tables of reference 3. Two samples of size distributions taken on different days and in different cloud formations are used in table II and are identified with the flight, run, and picture numbers given in reference 3. The droplets are distributed by size (diameter) into groups, each group except the first covering a size range of 5 microns. The inertia parameter K (row A) and free-stream Reynolds number Re_0 (row B) are calculated using the average diameter in the size group, except the first group for which a 5-micron diameter was used.

The number of droplets in each size group is given in rows C and J for flights 1 and 3, respectively, and the amount of water in each size group, as a fractional part of the total water measured in the cloud, is given in rows D and K. For example, for flight 1 slightly more than one-tenth of the total water measured in the cloud is contained in the 269 droplets in the 7.6-to-12.5-micron-diameter group. For flight 1 the rate of droplet collection is analyzed at five chordwise positions approximately 1 inch apart on the surface of the airfoil (rows E to I). For flight 3 the analysis is made at the stagnation line only (s = 0, row L). Each row gives the local collection efficiency β obtained from figures 12 and 13 and the product of β and the water contained in the size group (rows D and K for flights 1 and 3, respectively). For example, at the stagnation line (s = 0) for flight 1 the local collection efficiency is 0.19 for the 7.6- to 12.5-micron size group, and the product of β and the water contained in that size group is $0.19 \times 0.107 = 0.0203$. This value is the contribution by the 7.6- to 12.5-micron size group to a small segment of blotter located at the stagnation line. The summation of all the contributions at the stagnation line by all the size groups present in the cloud gives a local collection efficiency which is weighted according to the droplet size versus the water content distribution in the cloud. The local rate of water impingement is obtained when the weighted value of β is used in equation (11).

In the dye-tracer technique the problem is worked in the reverse order from that presented herein. The local rate of water impingement W_β is the quantity measured, and from W_β the droplet-size distribution is obtained (see appendix B). The examples in table II illustrate the sensitivity required in the dye-tracer technique in order to treat adequately size groups that make small contributions to the total effect. An error of -5 percent in β caused by errors in measurements of W_β is listed in each of the rows analyzed. The manner in which this error affects the droplet-size distribution and the liquid-water content is discussed in the text.

For the purpose of the example illustrating the masking effect, it is assumed that the data on size distribution and liquid-water content measured by the aeroscope are as accurate as needed here, and the values measured by the aeroscope are arbitrarily taken as the standards for comparison with an instrument which uses a Joukowski airfoil section (36.5 percent thick) as the collecting element.

REFERENCES

1. Brun, R. J., Lewis, W., Perkins, P. J., and Serafini, J. S.: Impingement of Cloud Droplets on a Cylinder and Procedure for Measuring Liquid-Water Content and Droplet Sizes in Supercooled Clouds by Rotating Multicylinder Method. NACA Rep. 1215, 1955. (Supersedes NACA TN's 2903, 2904, and NACA RM E53D23.)

2. von Glahn, Uwe H., Gelder, Thomas F., and Smyers, William H., Jr.: A Dye-Tracer Technique for Experimentally Obtaining Impingement Characteristics of Arbitrary Bodies and a Method for Determining Droplet Size Distribution. NACA TN 3338, 1955.

3. Hacker, Paul T.: An Oil-Stream Photomicrographic Aeroscope for Obtaining Cloud Liquid-Water Content and Droplet Size Distribution in Flight. NACA TN 3592, 1956.

4. Brun, Rinaldo J., Gallagher, Helen M., and Vogt, Dorothea E.: Impingement of Water Droplets on NACA 65_1-208 and 65_1-212 Airfoils at 4° Angle of Attack. NACA TN 2952, 1953.

5. Langmuir, Irving, and Blodgett, Katherine B.: A Mathematical Investigation of Water Droplet Trajectories. Tech. Rep. No. 5418, Air Materiel Command, AAF, Feb. 19, 1946. (Contract No. W-33-038-ac-9151 with General Electric Co.)

6. Brun, Rinaldo J., and Mergler, Harry W.: Impingement of Water Droplets on a Cylinder in an Incompressible Flow Field and Evaluation of Rotating Multicylinder Method for Measurement of Droplet-Size Distribution, Volume-Median Droplet Size, and Liquid-Water Content in Clouds. NACA TN 2904, 1953.

7. Glauert, H.: The Elements of Aerofoil and Airscrew Theory. The
   Macmillan Co. (New York), 1944.

8. Guibert, A. G., Janssen, E., and Robbins, W. M.: Determination of
   Rate, Area, and Distribution of Impingement of Waterdrops on Various
   Airfoils from Trajectories Obtained on the Differential Analyzer.
   NACA RM 9A05, 1949.

9. Sherman, P., Klein, J. S., and Tribus, M.: Determination of Drop
   Trajectories by Means of an Extension of Stokes' Law. Eng. Res.
   Inst., Univ. Mich., Apr. 1952. (Air Res. and Dev. Command, USAF,
   Contract AF 18(600)-51, Proj. M992-D.)

10. Gelder, Thomas F., Smyers, William H., Jr., and von Glahn, Uwe: Ex-
    perimental Droplet Impingement on Several Two-Dimensional Airfoils
    with Thickness Ratios of 6 to 16 Percent. NACA TN 3839, 1956.

11. Davies, C. N., and Peetz, C. V.: Impingement of Particles on a
    Transverse Cylinder. Proc. Roy. Soc., (London), ser. A, vol. 234,
    no. 1197, Feb. 7, 1956, pp. 269-295.

12. von Glahn, Uwe H.: Use of Truncated Flapped Airfoils for Impingement
    and Icing Tests of Full-Scale Leading-Edge Sections. NACA RM
    E56E11, 1956.

4016

CJ-4

TABLE I. - COORDINATE POINTS FOR SYMMETRICAL

36.5-PERCENT JOUKOWSKI AIRFOIL

x	y	s	x	y	s
0	0	0	0.2803	0.1818	0.368
.0024	.0248	.025	.2884	.1817	.376
.0095	.0492	.050	.3713	.1752	.458
.021	.0726	.078	.4563	.1594	.548
.0372	.0945	.104	.5408	.1369	.633
.0575	.1146	.132	.6229	.1106	.723
.0816	.1325	.161	.7008	.0834	.800
.1094	.1479	.194	.7729	.0580	.879
.1404	.1606	.227	.8376	.0364	.948
.1741	.1704	.262	.8934	.0199	1.003
.1884	.1734	.275	.9388	.0088	1.049
.2029	.1760	.291	.9724	.0027	1.082
.2104	.1771	.299	.9931	.0004	1.103
.2400	.1810	.328	1.0000	0	1.110

TABLE II. - EXAMPLE ILLUSTRATING MASKING EFFECT

[Flight speed, 200 mph; altitude, 10,000 ft; airfoil chord length, 18 in]

Identification in ref. 3	Cloud type	Measured liquid-water content, g/cu m	Volume-median droplet diameter, microns	Droplet parameters and surface position		Row identification	Local collection efficiency, β, and size contribution	Droplet-size range, microns											Weighted local collection efficiency	Magnitude of 5-percent error in β weighted
								0 - 7.5	7.6 - 12.5	12.6 - 17.5	17.6 - 22.5	22.6 - 27.5	27.6 - 32.5	32.6 - 37.5	37.6 - 42.5	42.6 - 47.5	47.6 - 52.5	52.6 - 57.5		
Flight 1, run 5, picture 5	Cumulus congestus	1.7	19.4	Inertia parameter, K	A			0.016	0.066	0.15	0.26	0.41	0.59	0.81	1.05	1.35	1.64	1.99		
				Free-stream Reynolds number, Re_0	B			25	50	75	100	125	150	175	200	225	250	275		
				Number of droplets	C			97	269	203	84	15	1	2	1	2	1	1		
				Water contained in size group, fraction of total	D			0.005	0.107	0.272	0.266	0.095	0.011	0.034	0.025	0.072	0.049	0.066		
				Surface position, s	0	E	β	0.03	0.19	0.49	0.54	0.51	0.65	0.69	0.72	0.74	0.79	0.81	0.5482	0.0274
							Size contribution	0.0002	0.0203	0.1333	0.1438	0.0587	0.0071	0.0235	0.0180	0.0532	0.0387	0.0534		
					0.066	F	β	0	0	0.30	0.39	0.46	0.53	0.57	0.60	0.67	0.69	0.72	0.3977	0.0199
							Size contribution	------	------	0.0816	0.1038	0.0427	0.0058	0.0194	0.0150	0.0482	0.0338	0.0475		
					0.111	G	β	0	0	0	0.09	0.23	0.32	0.40	0.39	0.48	0.50	0.54	0.1868	0.0083
							Size contribution	------	------	------	0.0239	0.0214	0.0055	0.0136	0.0097	0.0346	0.0245	0.0356		
					0.166	H	β	0	0	0	0	0	0.04	0.16	0.15	0.24	0.23	0.30	0.0619	0.0005
							Size contribution	------	------	------	------	------	0.0044	0.0054	0.0037	0.0173	0.0113	0.0198		
					0.222	I	β	0	0	0	0	0	0	0	0	0	0.04	0.07	0.0066	0.0000
							Size contribution	------	------	------	------	------	------	------	------	------	0.0020	0.0046		
Flight 3, run 3, picture 2	Strato-cumulus	0.17	11.3	Number of droplets	J			88	139	16	2									
				Water contained in size group, fraction of total	K			0.049	0.633	0.245	0.073									
				Surface position, s	0	L	β	0.03	0.19	0.49	0.54								0.2811	0.0141
							Size contribution	0.0015	0.1202	0.1200	0.0394									
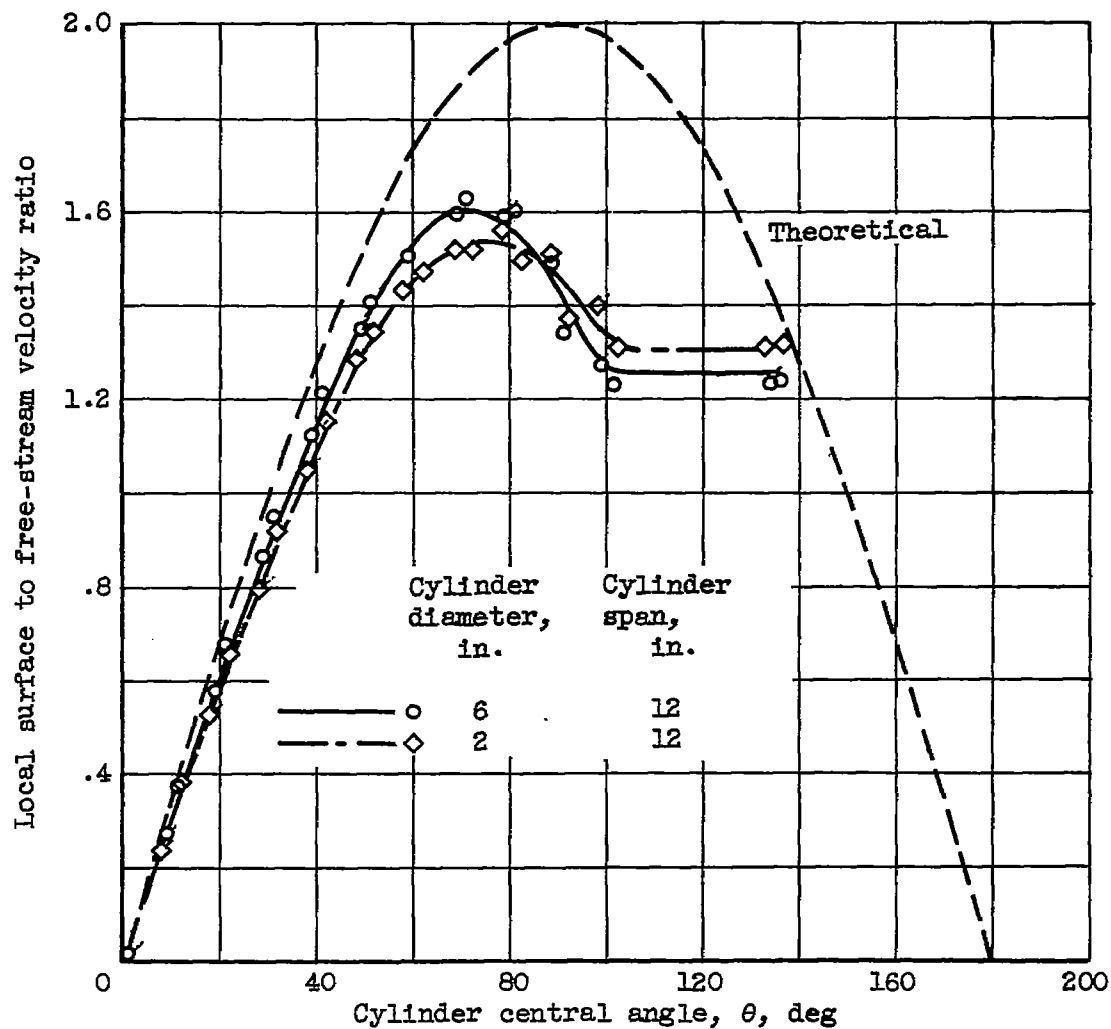
Figure 1. - Comparison of experimental (icing tunnel) with
theoretical surface to free-stream velocity ratio for 6- and
2-inch-diameter cylinders (ref. 2). Free-stream velocity,
175 miles per hour.
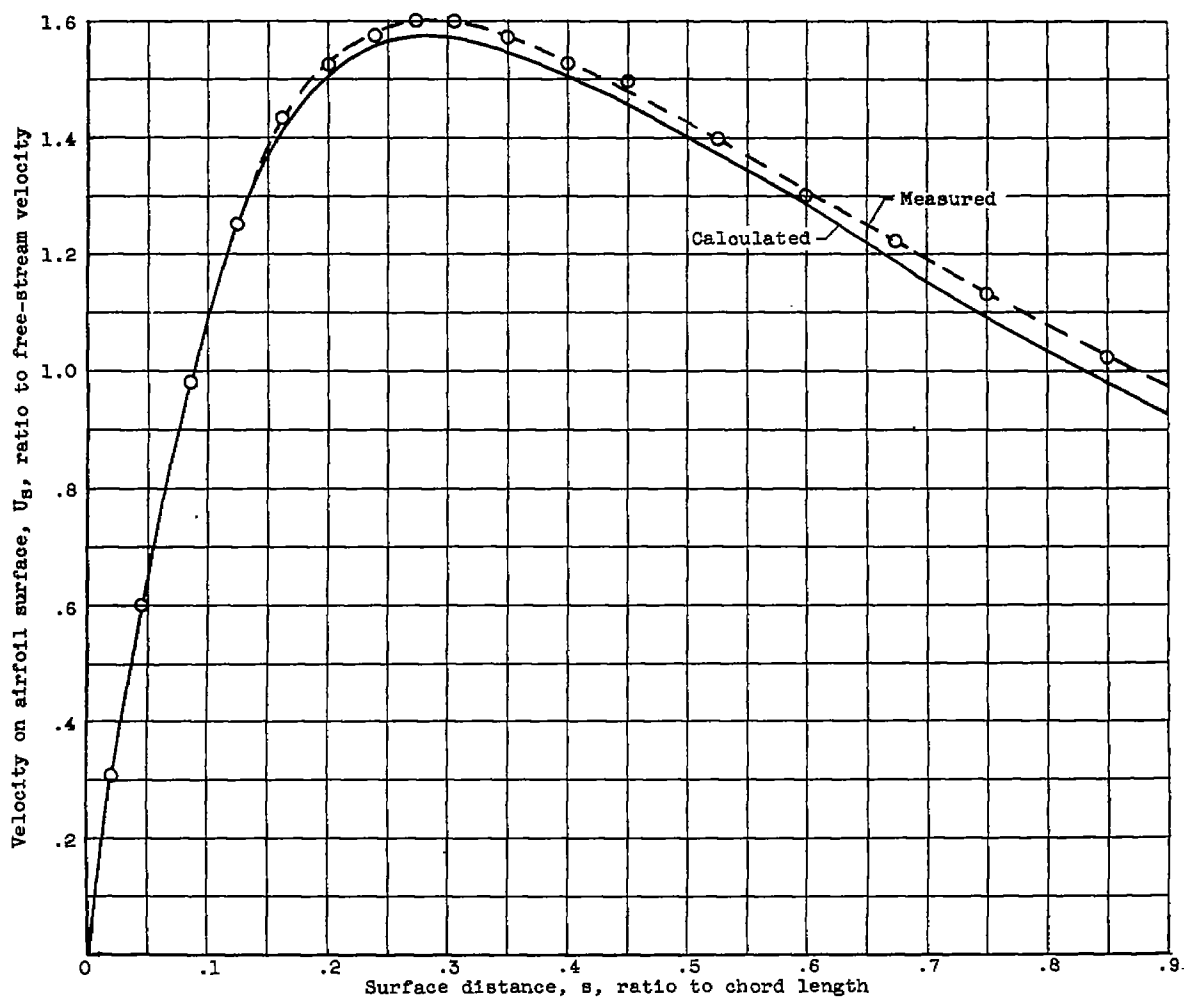
Figure 2. - Comparison of experimental (icing tunnel) with theoretical surface to free-stream velocity ratio for 36.5-percent-thick symmetrical Joukowski airfoil. Angle of attack, 0°; tunnel airspeed, 175 miles per hour; airfoil chord length, 16.32 inches.
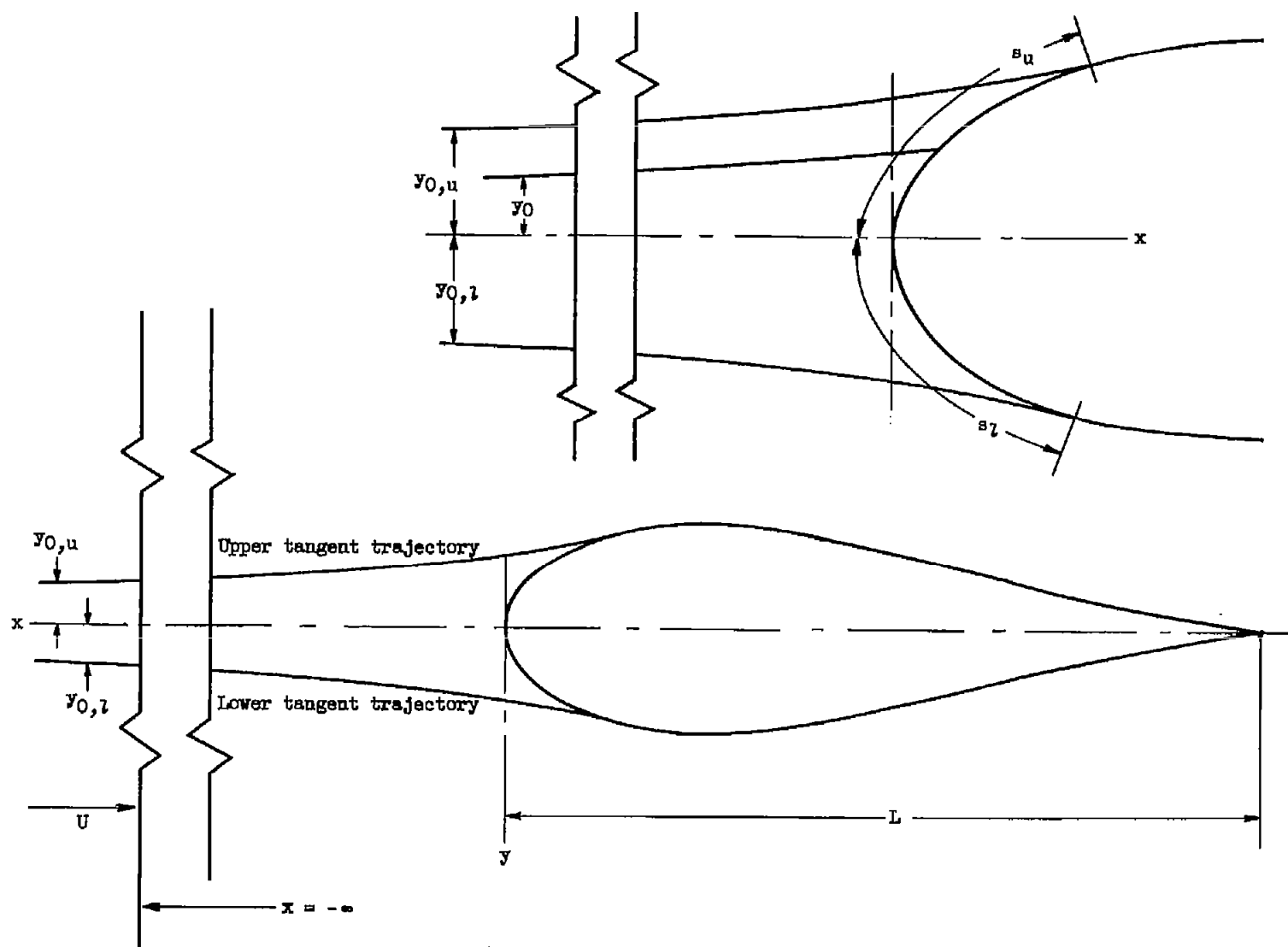
Figure 3. - Droplet trajectories with respect to airfoil.
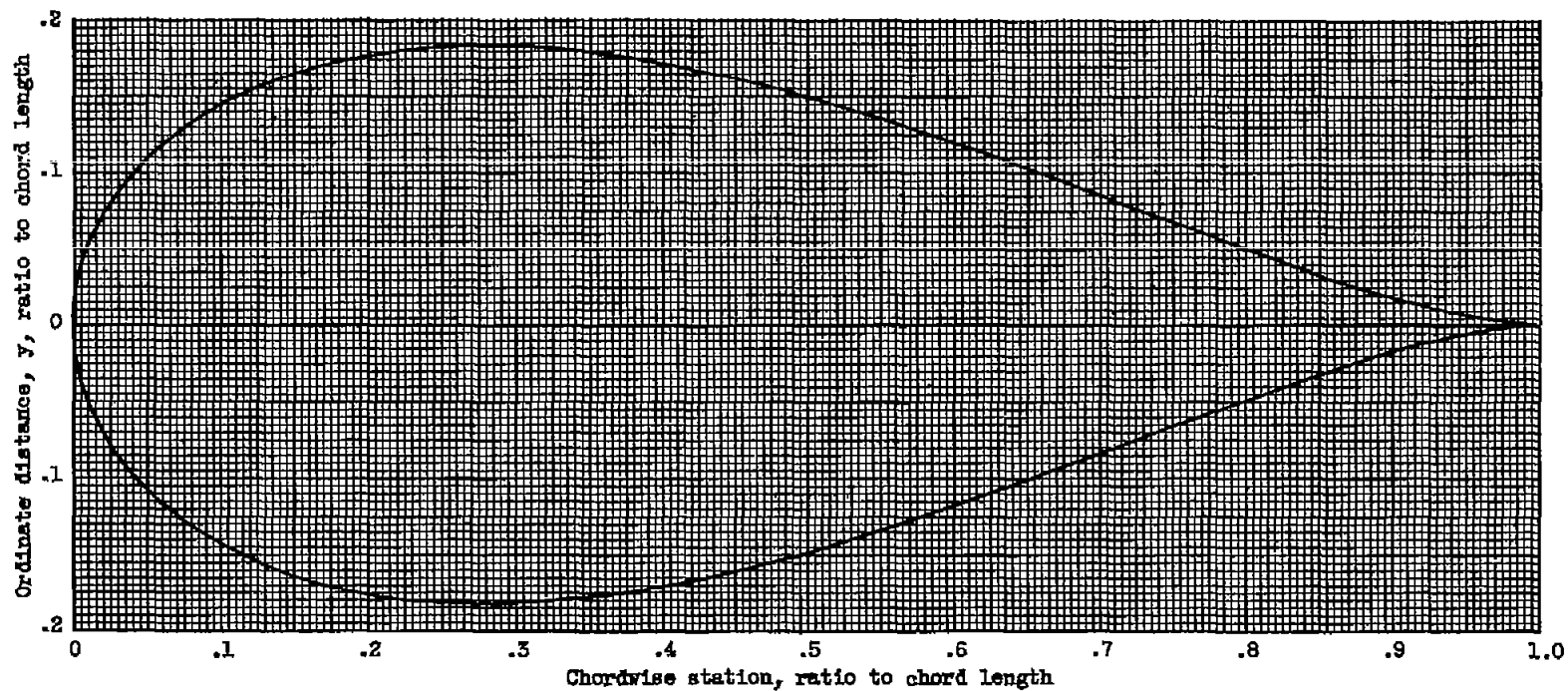
Figure 4. - Geometric shape of 36.5-percent-thick Joukowski airfoil.
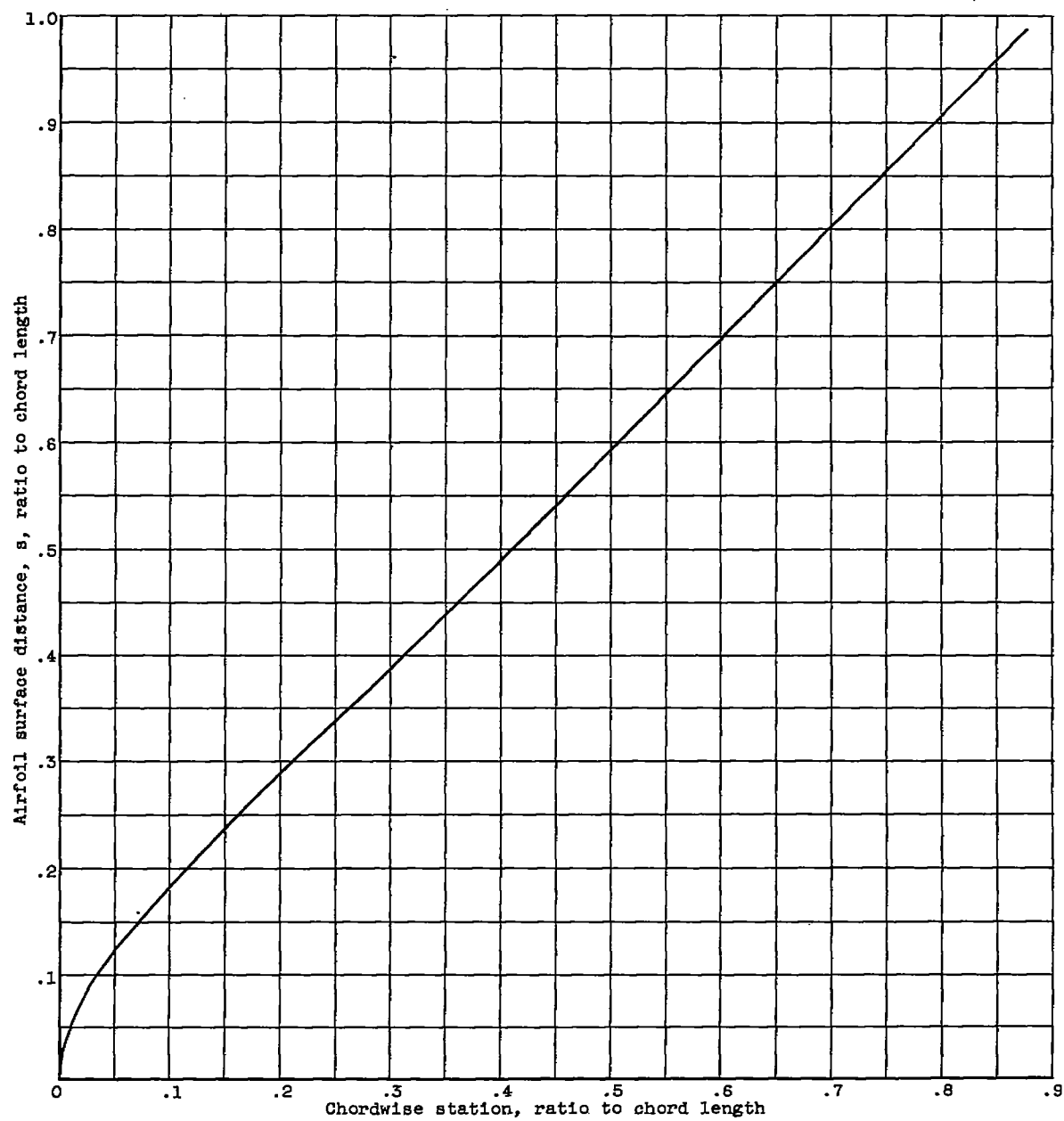
Figure 5. - Relation between distance along surface of 36.5-percent-thick Joukowski airfoil and chordwise station.
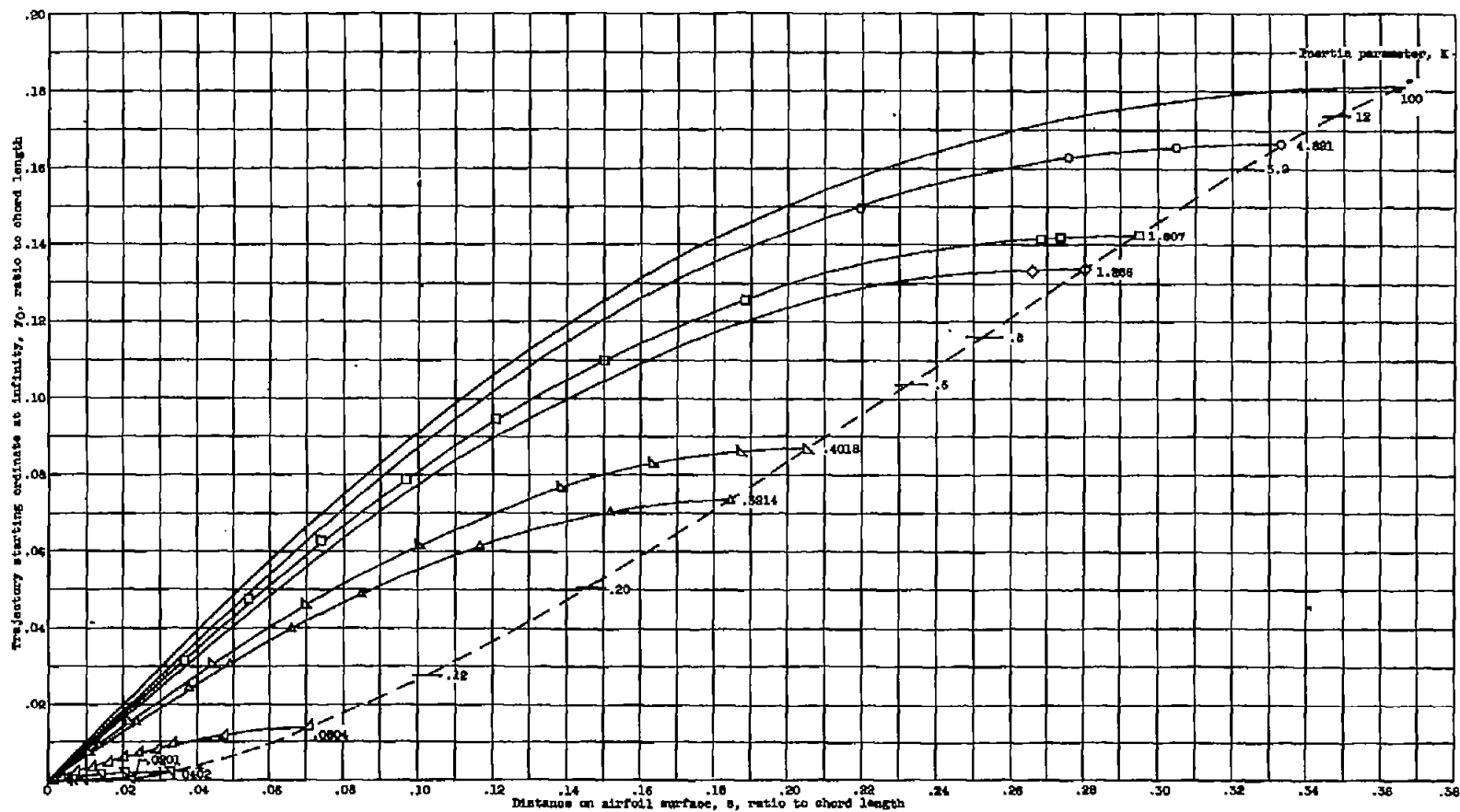
(a) Free-stream Reynolds number, 16.

Figure 6. - Trajectory starting ordinates as function of point of impingement on surface of 36.5-percent-thick Joukowski airfoil. Angle of attack, 0°.
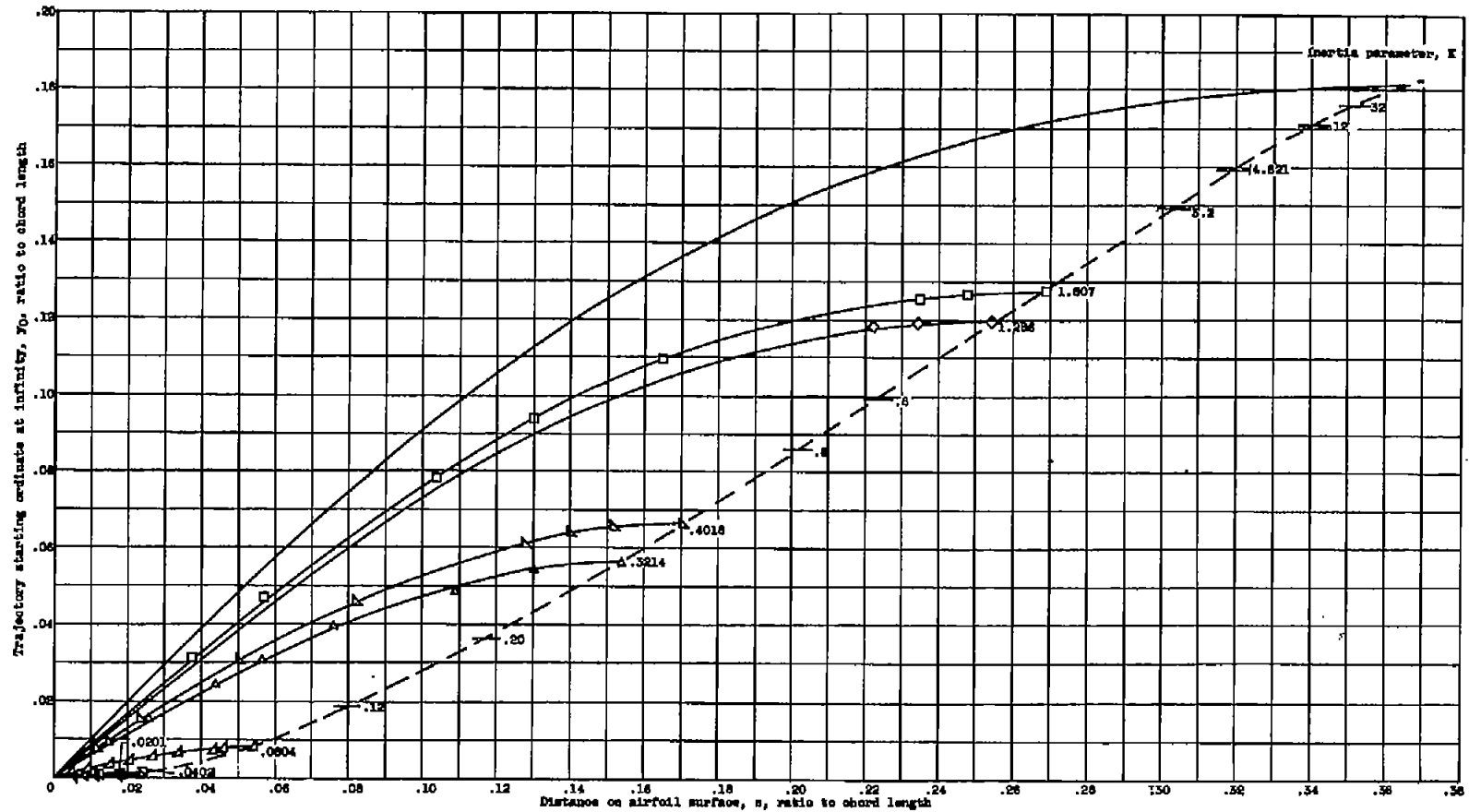
(b) Free-stream Reynolds number, 64.

Figure 8. - Continued. Trajectory starting ordinates as function of point of impingement on surface of 36.5-percent-thick Joukowski airfoil. Angle of attack, 0°.
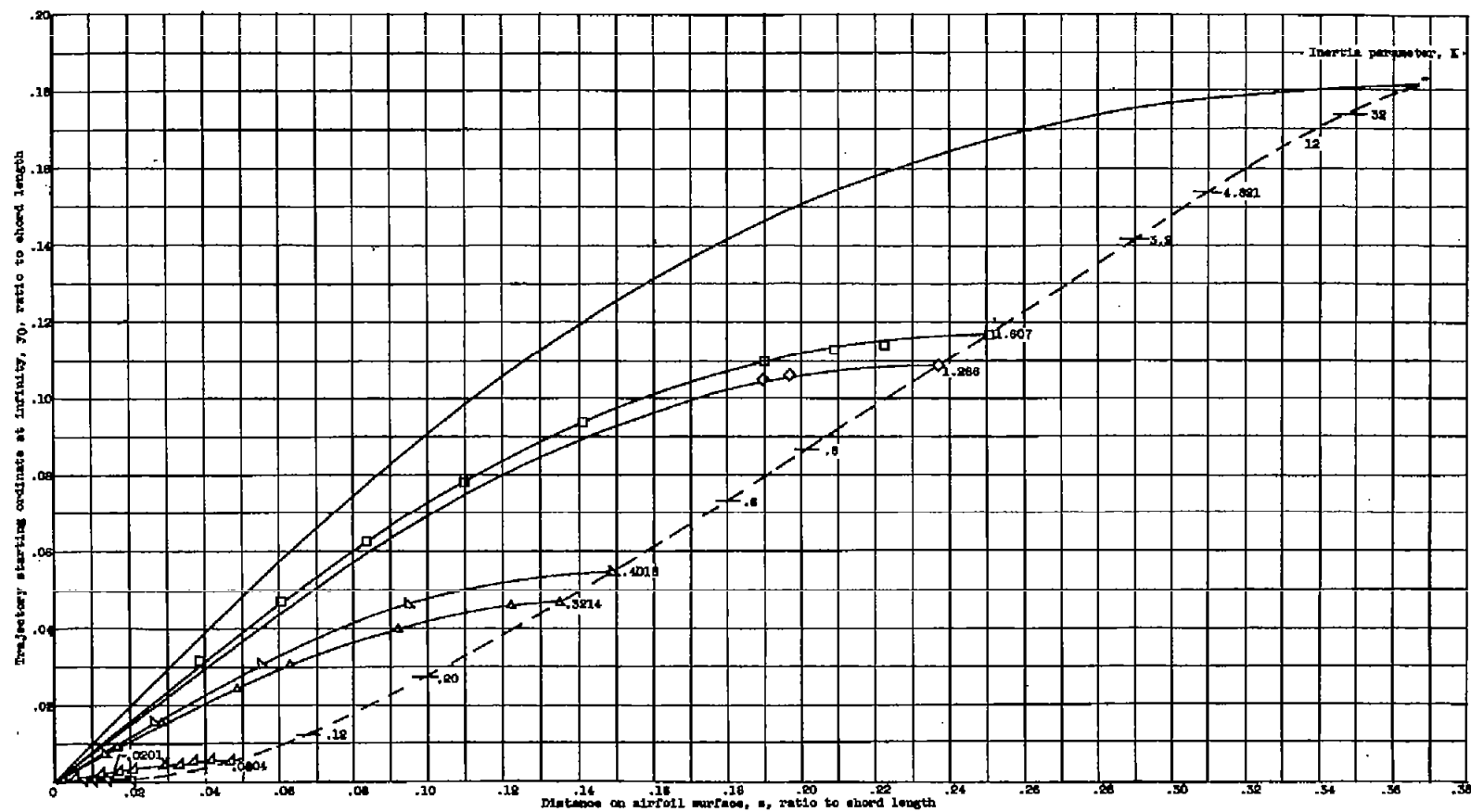
(c) Free-stream Reynolds number, 128.

Figure 6. - Continued. Trajectory starting ordinates as function of point of impingement on surface of 36.5-percent-thick Joukowski airfoil. Angle of attack, 0°.
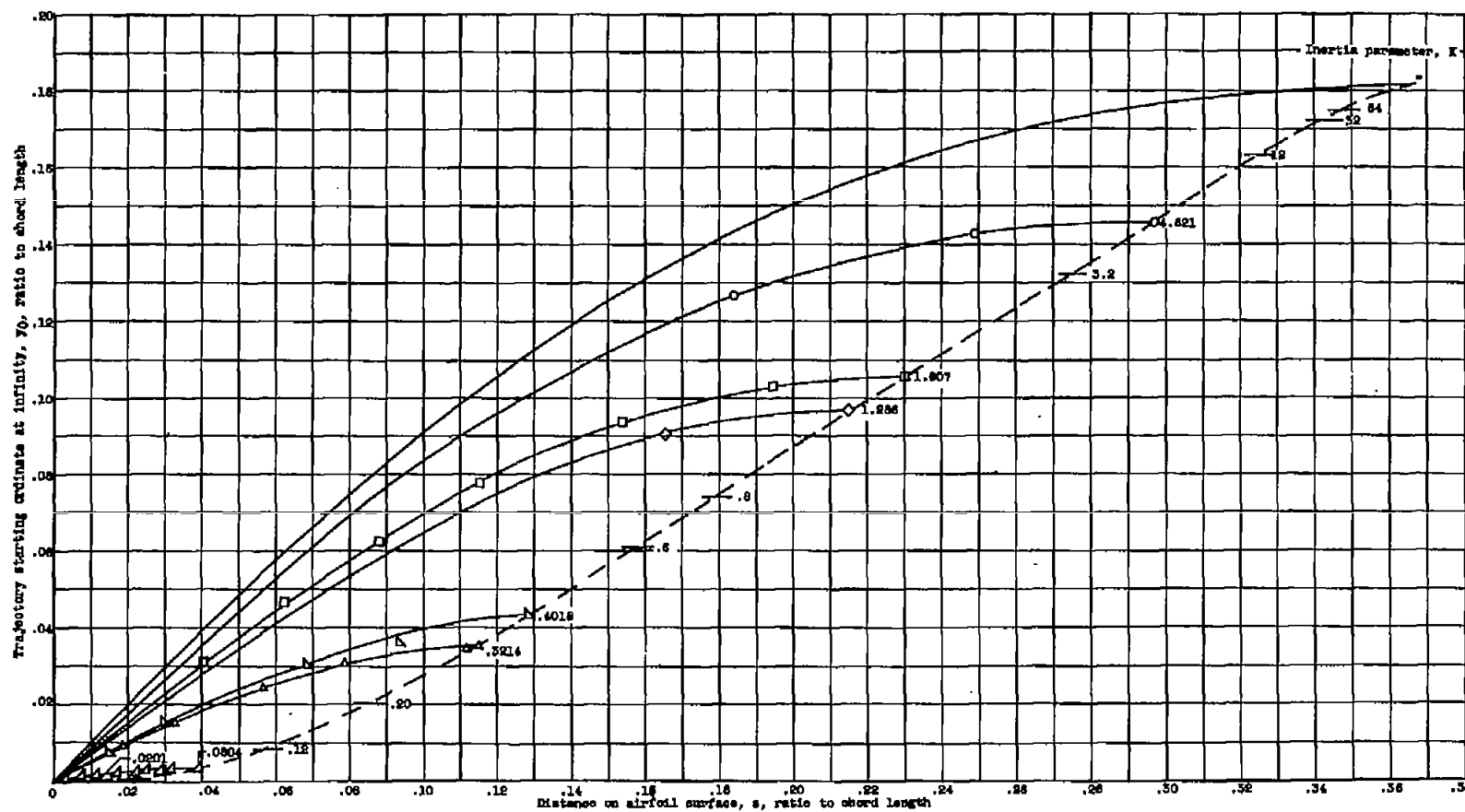
(d) Free-stream Reynolds number, 256.

Figure 6. - Continued. Trajectory starting ordinates as function of point of impingement on surface of 36.5-percent-thick Joukowski airfoil. Angle of attack, 0°.
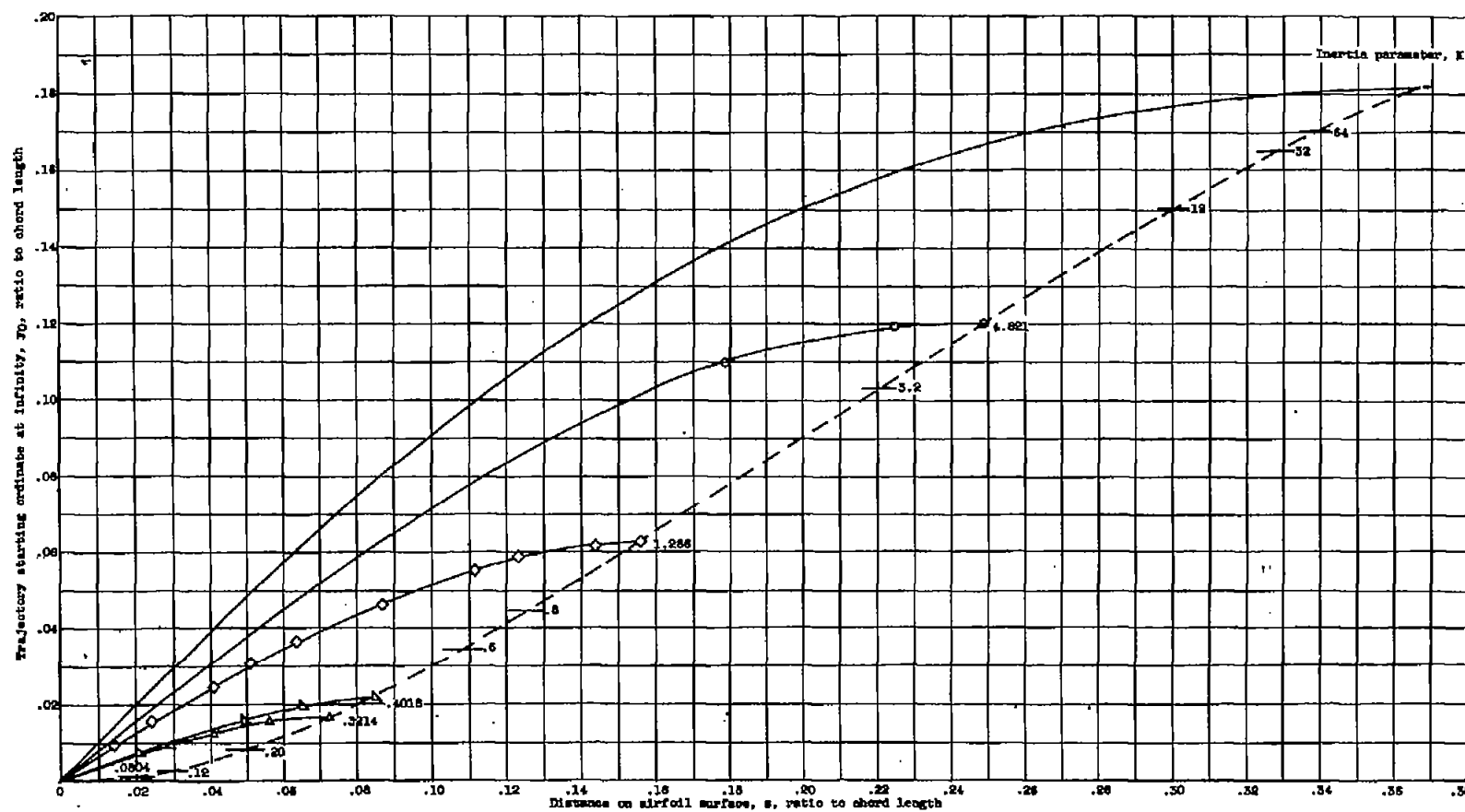
(e) Free-stream Reynolds number, 1024.

Figure 6. - Concluded. Trajectory starting ordinates as function of point of impingement on surface of 36.5-percent-thick Joukowski airfoil. Angle of attack, 0°.

4016

(c) Inertia parameter, 0.02008.
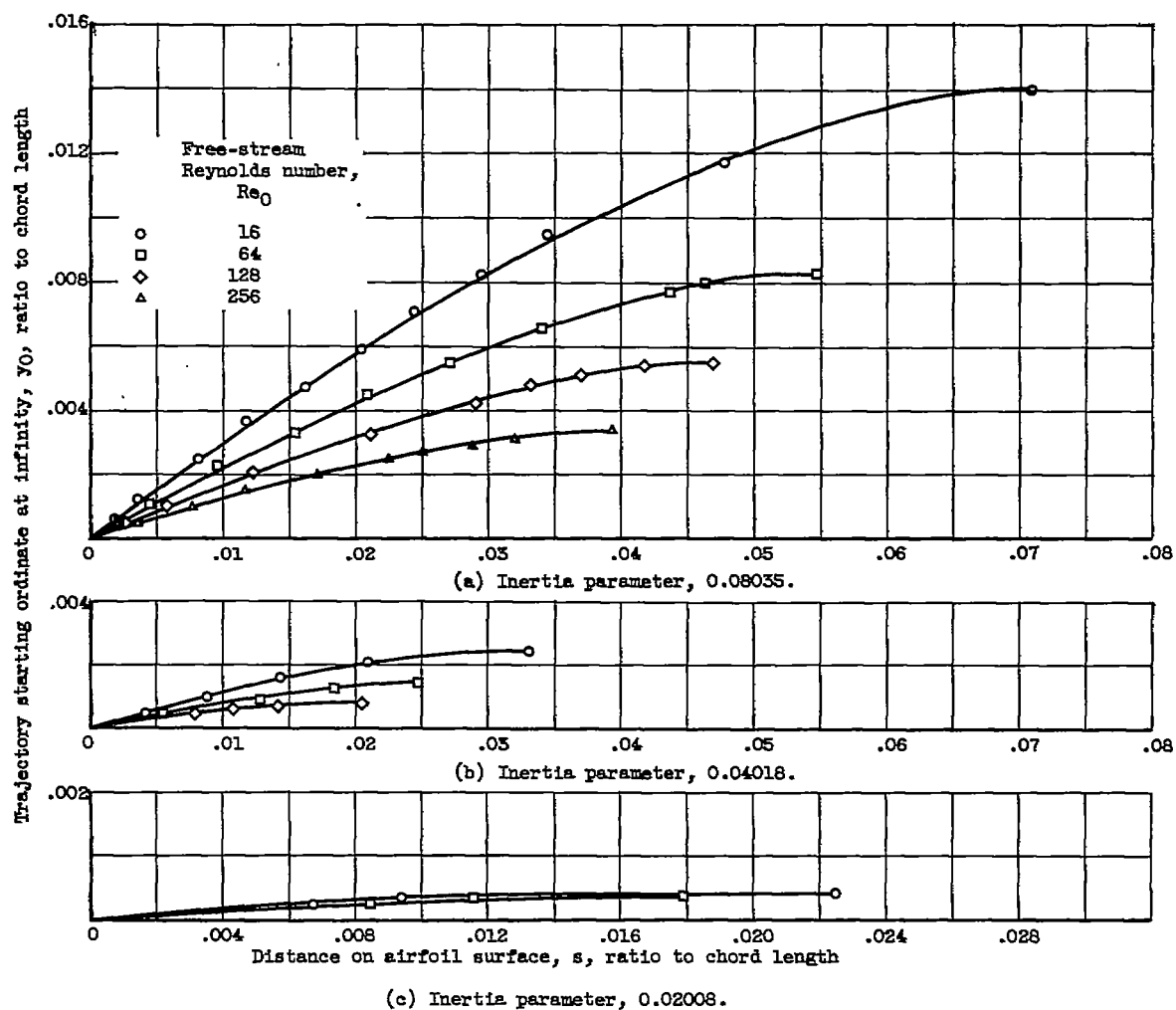
Figure 7. - Trajectory starting ordinates as function of point of impingement on airfoil surface for small values of inertia parameter. Angle of attack, 0°; 36.5-percent-thick Joukowski airfoil.
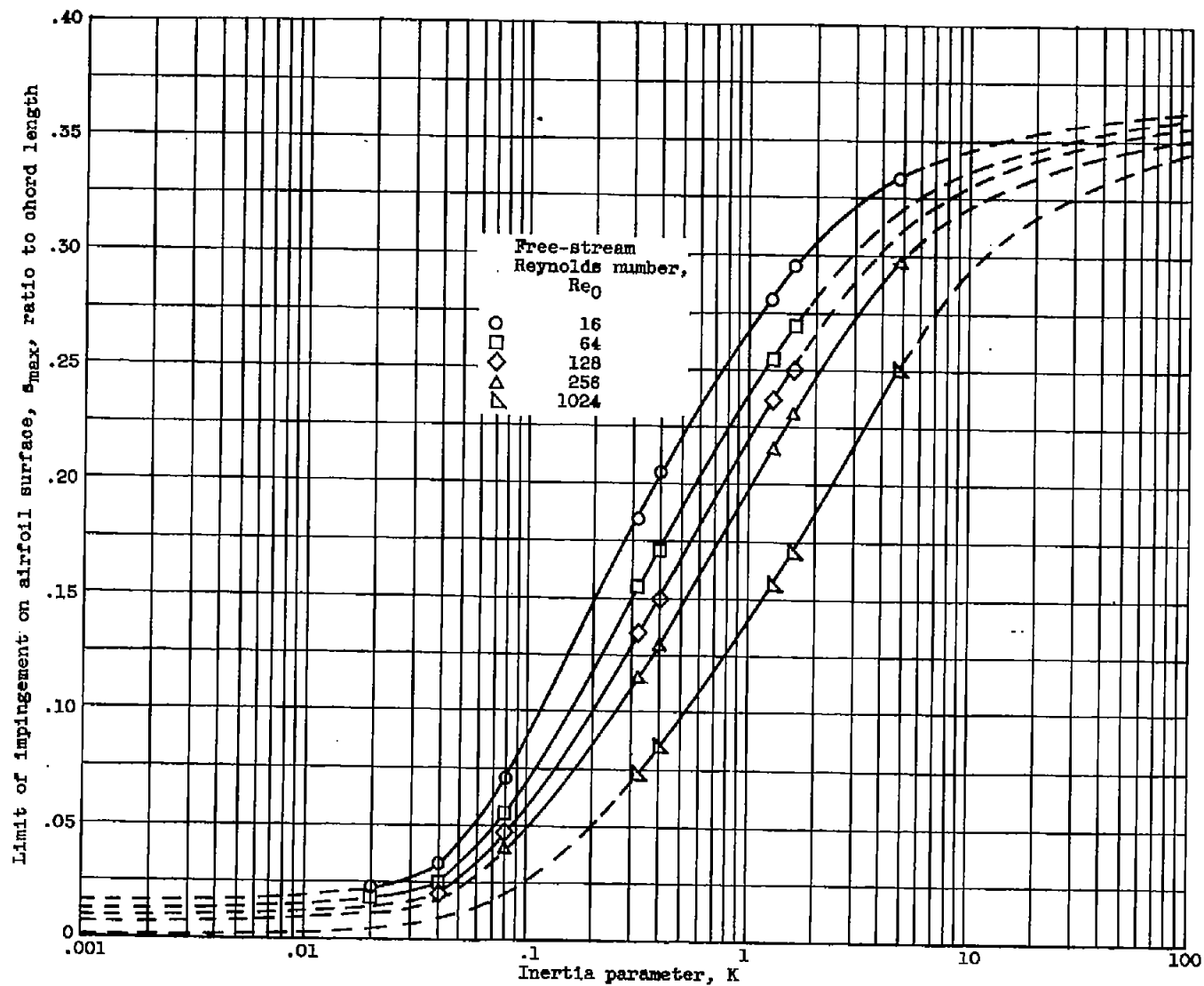
Figure 8. - Limit of impingement on upper or lower surface of 36.5-percent-thick Joukowski airfoil as function of inertia parameter and free-stream Reynolds number. Angle of attack, $0°$.
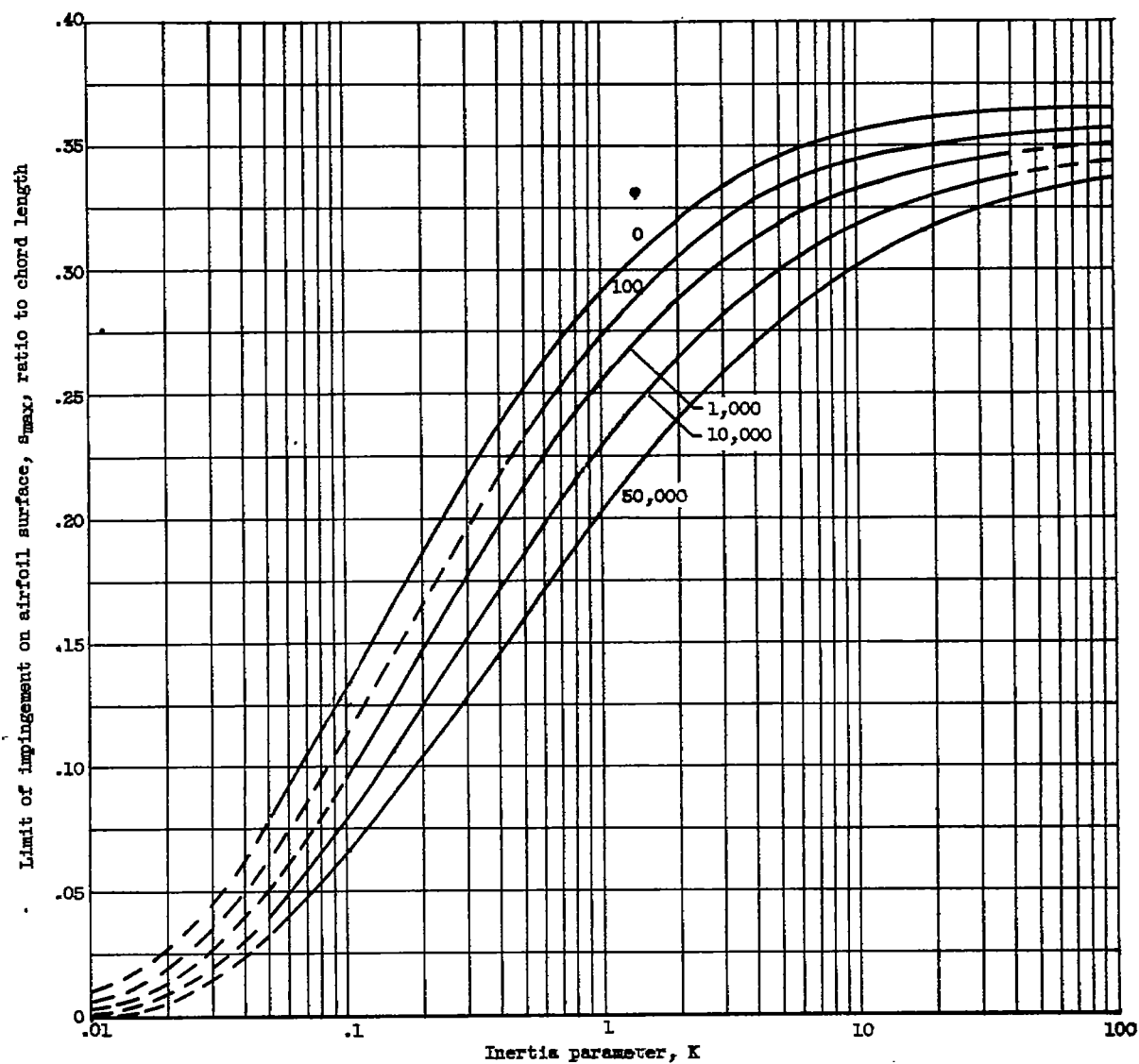
Figure 9. - Limit of impingement on upper or lower surface of 36.5-percent-thick Joukowski airfoil as function of inertia parameter and φ. Angle of attack, 0°.
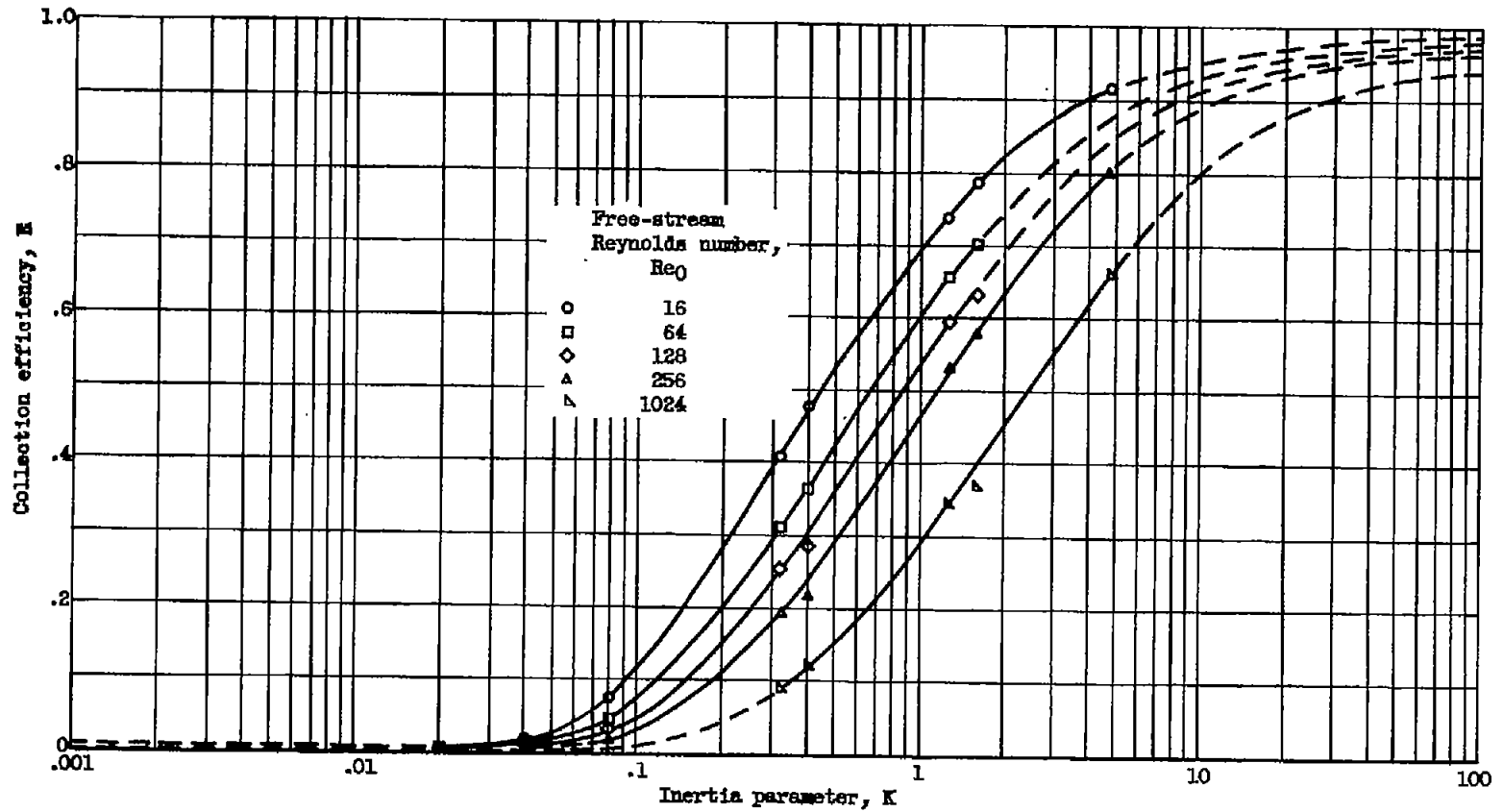
Figure 10. – Collection efficiency of 36.5-percent-thick Joukowski airfoil as function of inertia parameter and Reynolds number. Angle of attack, 0°.
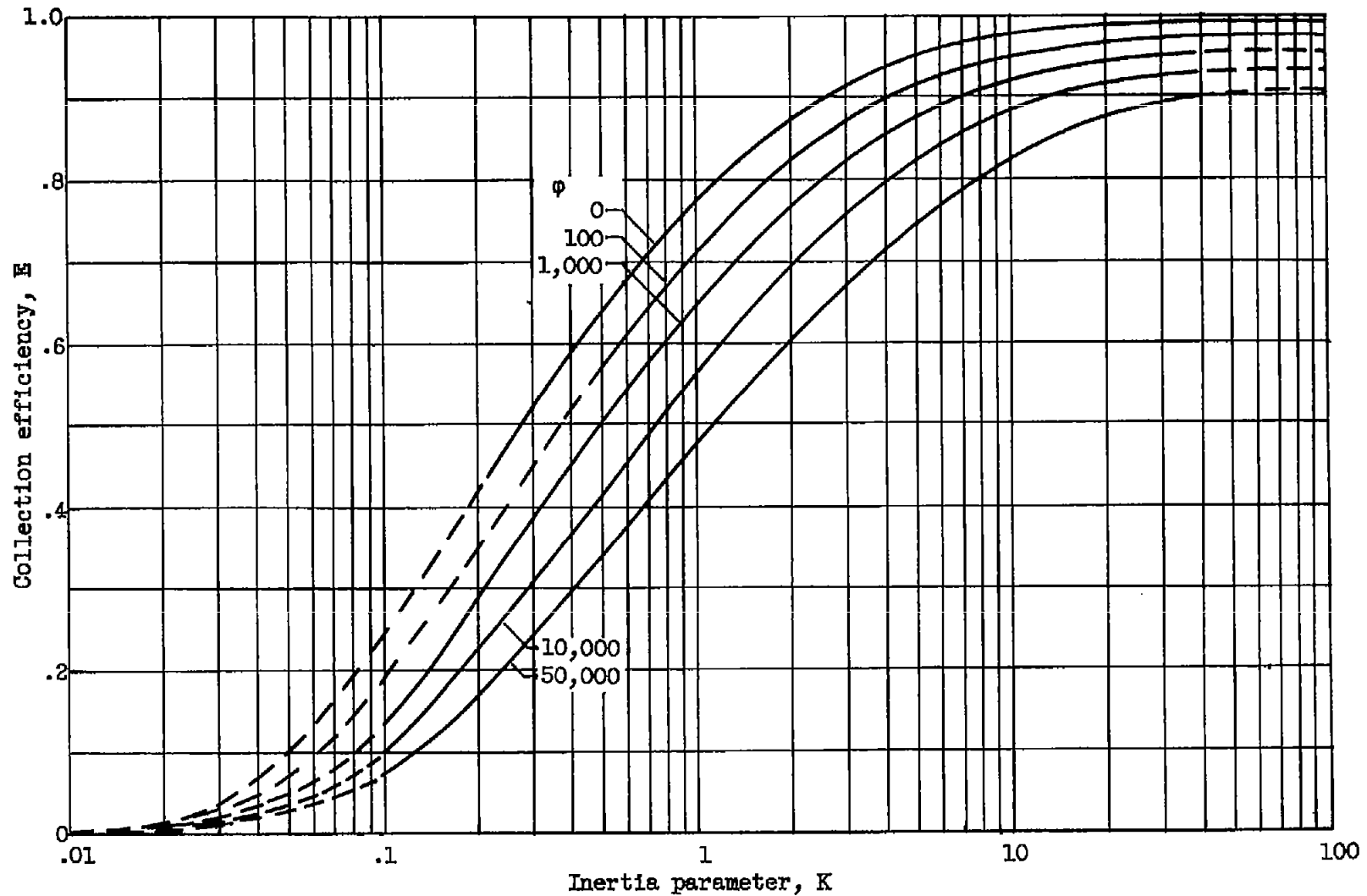
Figure 11. - Collection efficiency of 36.5-percent-thick Joukowski airfoil as function of inertia parameter and φ. Angle of attack, 0°.
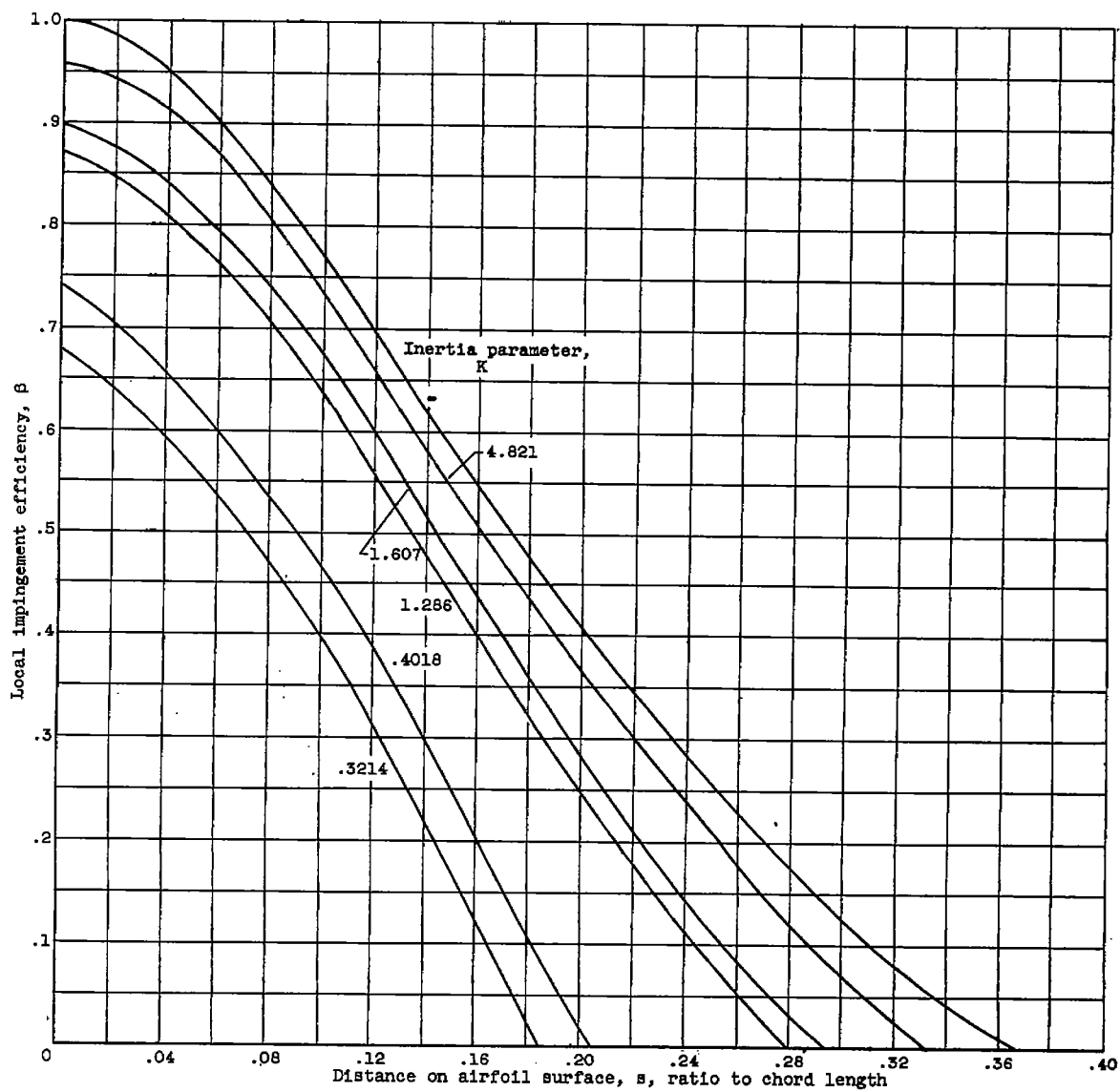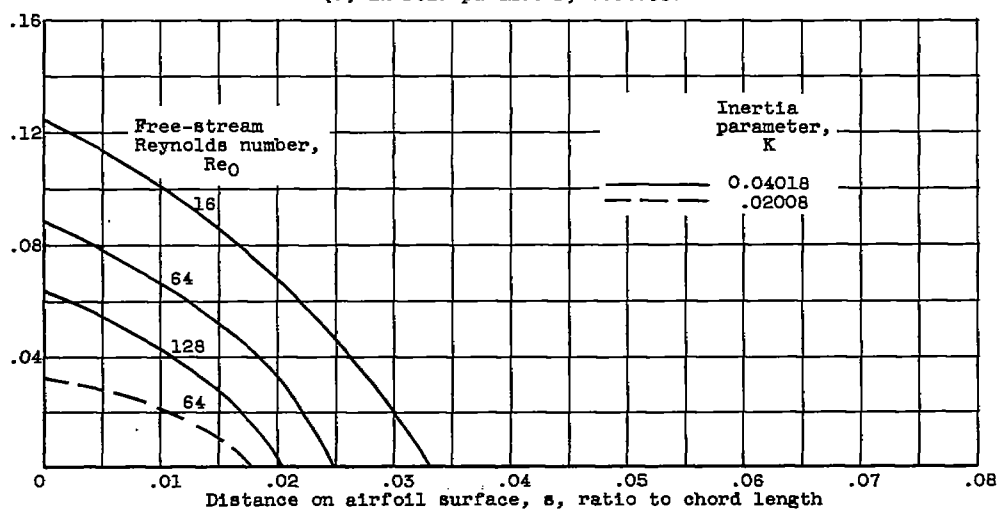
(a) Free-stream Reynolds number, 16.

Figure 12. – Local impingement efficiency on surface of 36.5-percent-thick Joukowski airfoil. Angle of
      attack, 0°.

CJ-6 back   4016

(b) Free-stream Reynolds number, 64.
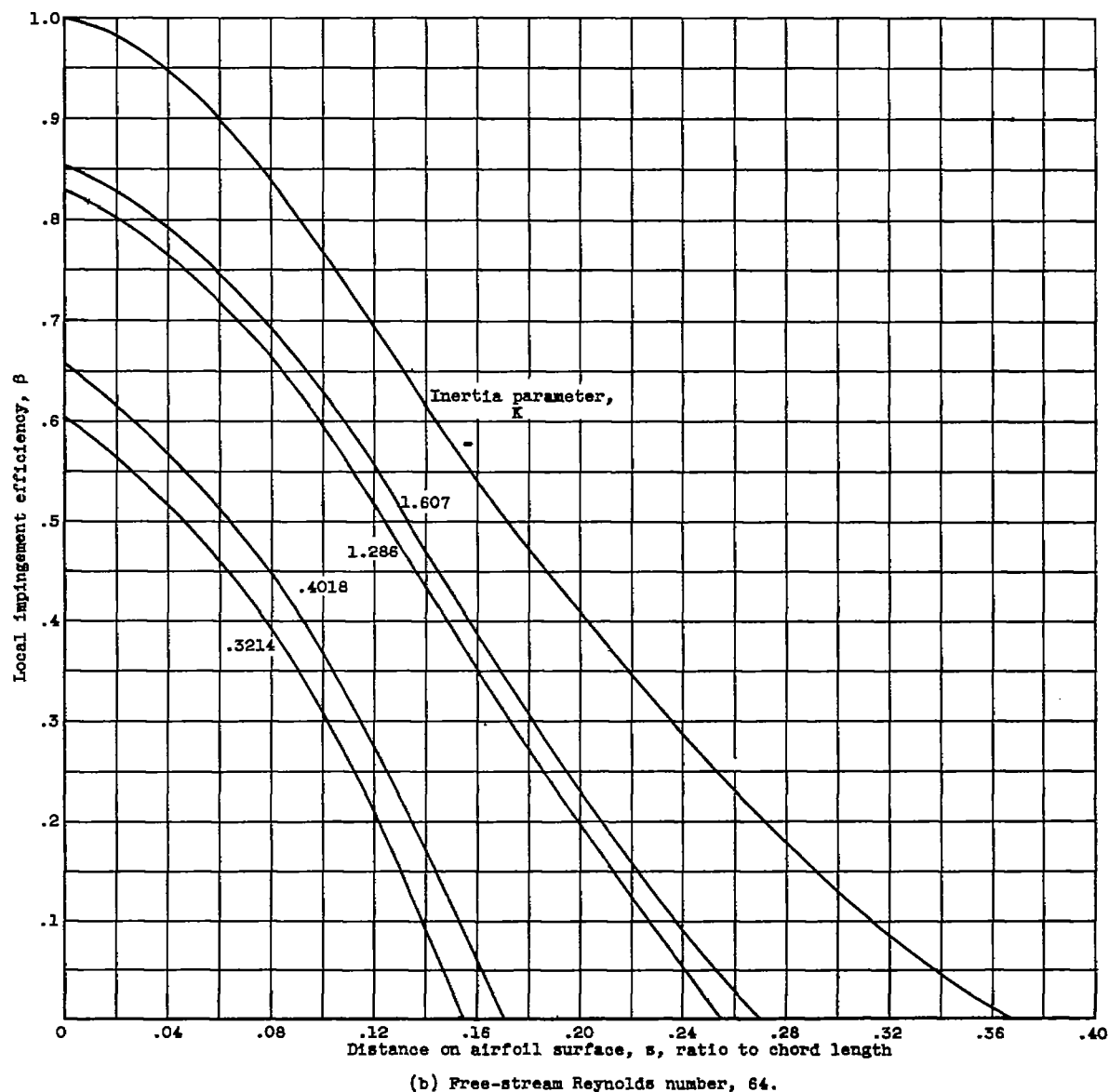
Figure 12. - Continued. Local impingement efficiency on surface of 36.5-percent-thick Joukowski air-
foil. Angle of attack, 0°.
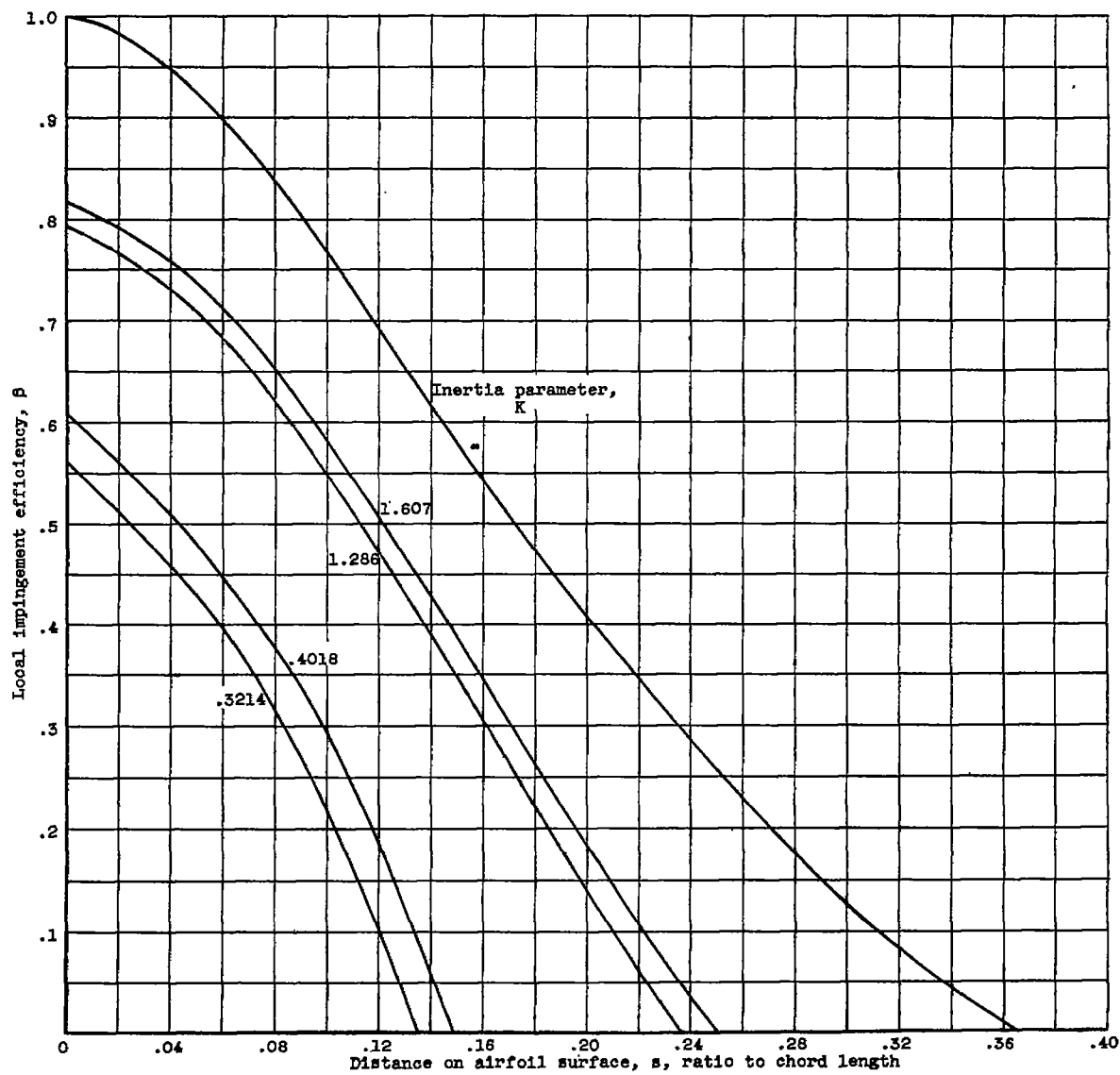
(c) Free-stream Reynolds number, 128.

Figure 12. - Continued. Local impingement efficiency on surface of 36.5-percent-thick Joukowski air-
foil. Angle of attack, 0°.

4016
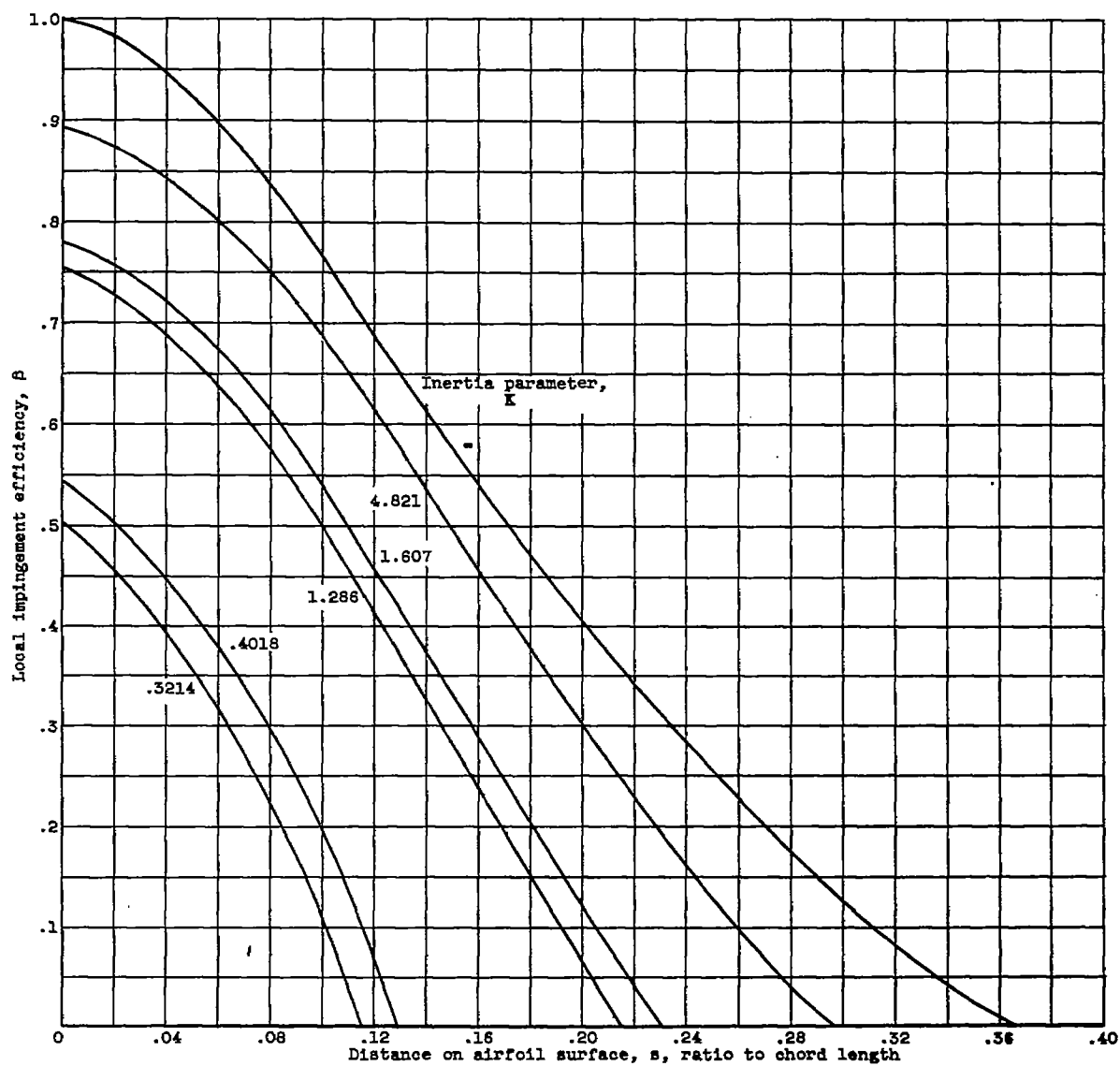
(d) Free-stream Reynolds number, 256.

Figure 12. - Continued. Local impingement efficiency on surface of 36.5-percent-thick Joukowski air-
foil. Angle of attack, 0°.
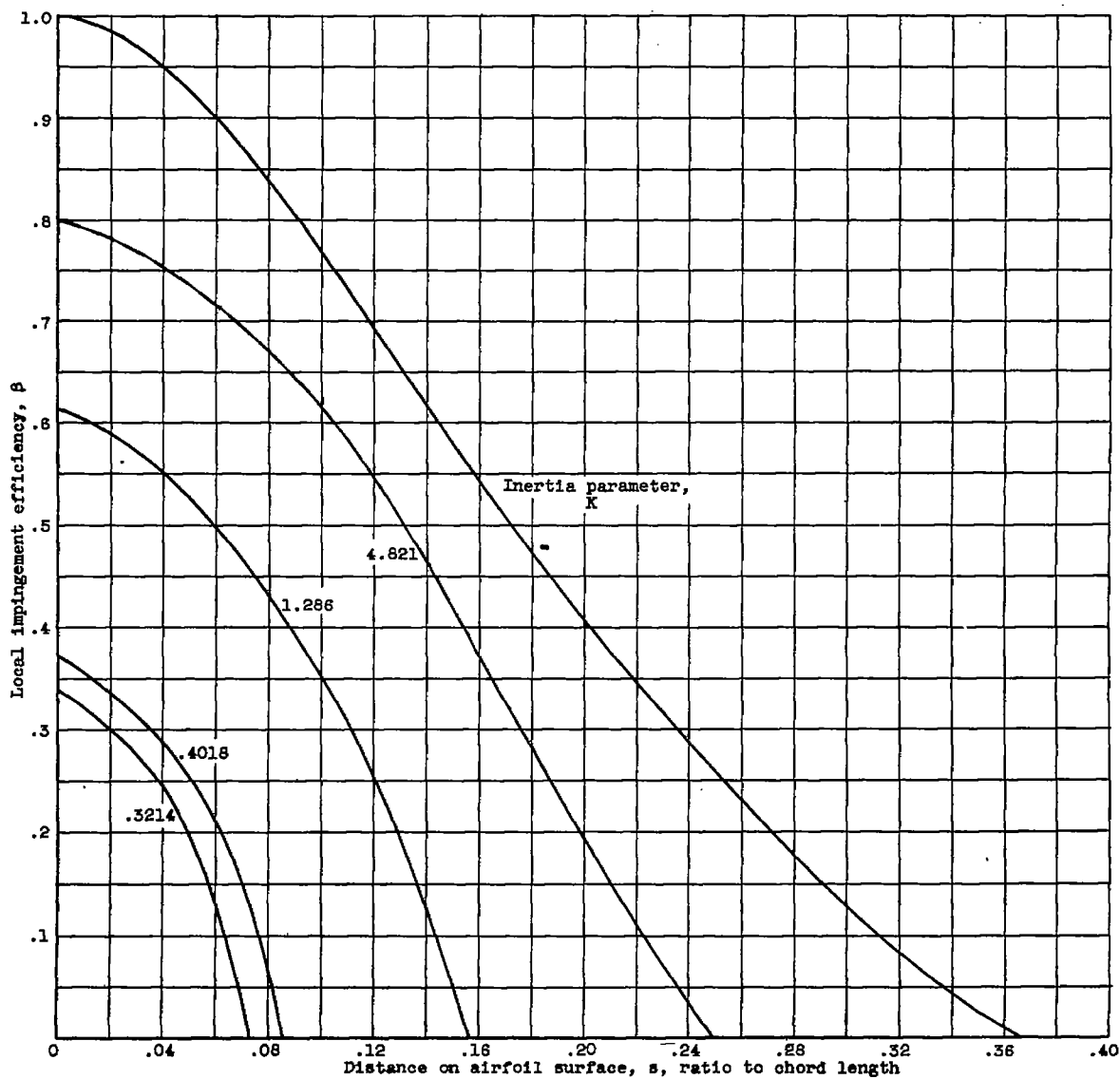
(e) Free-stream Reynolds number, 1024.

Figure 12. - Concluded. Local impingement efficiency on surface of 36.5-percent-thick Joukowski air-flow. Angle of attack, 0°.

4016
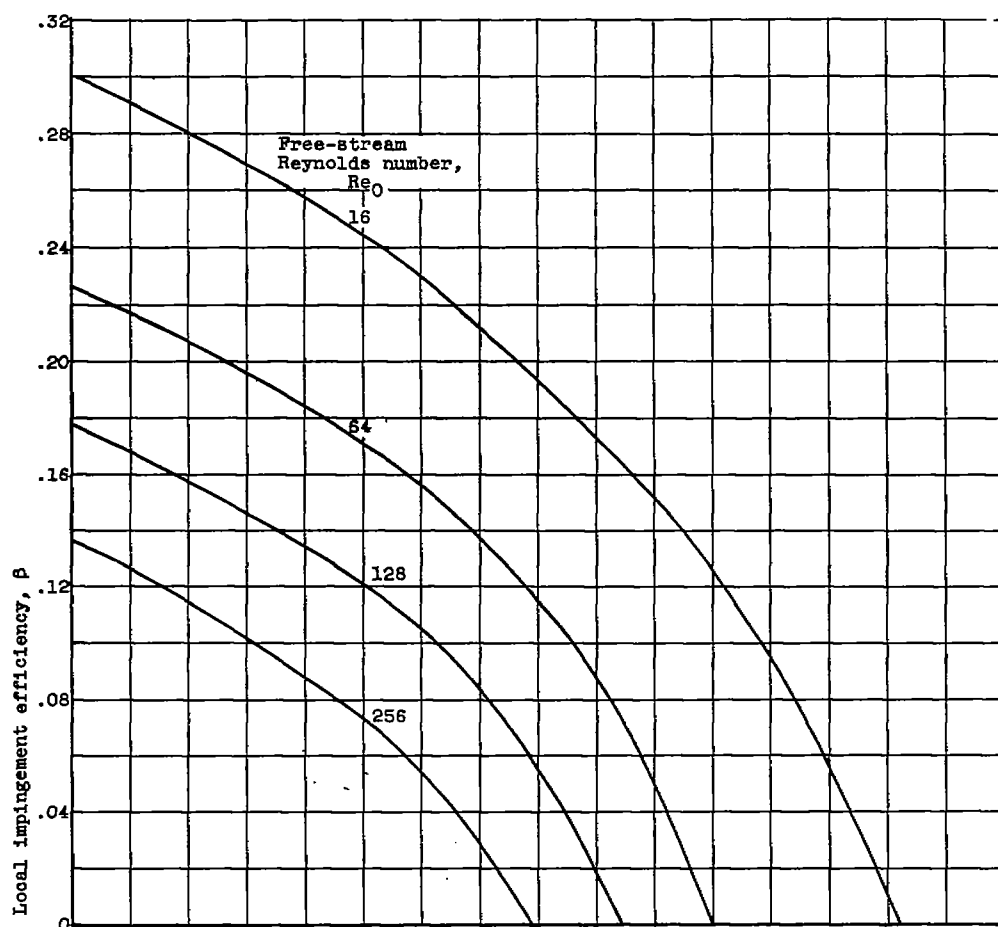
(a) Inertia parameter, 0.08035.

(b) Inertia parameter, 0.04018 and 0.02008.

Figure 13. - Local impingement efficiency on surface of 36.5-percent-thick Joukowski airfoil for low values of inertia parameter. Angle of attack, 0°.
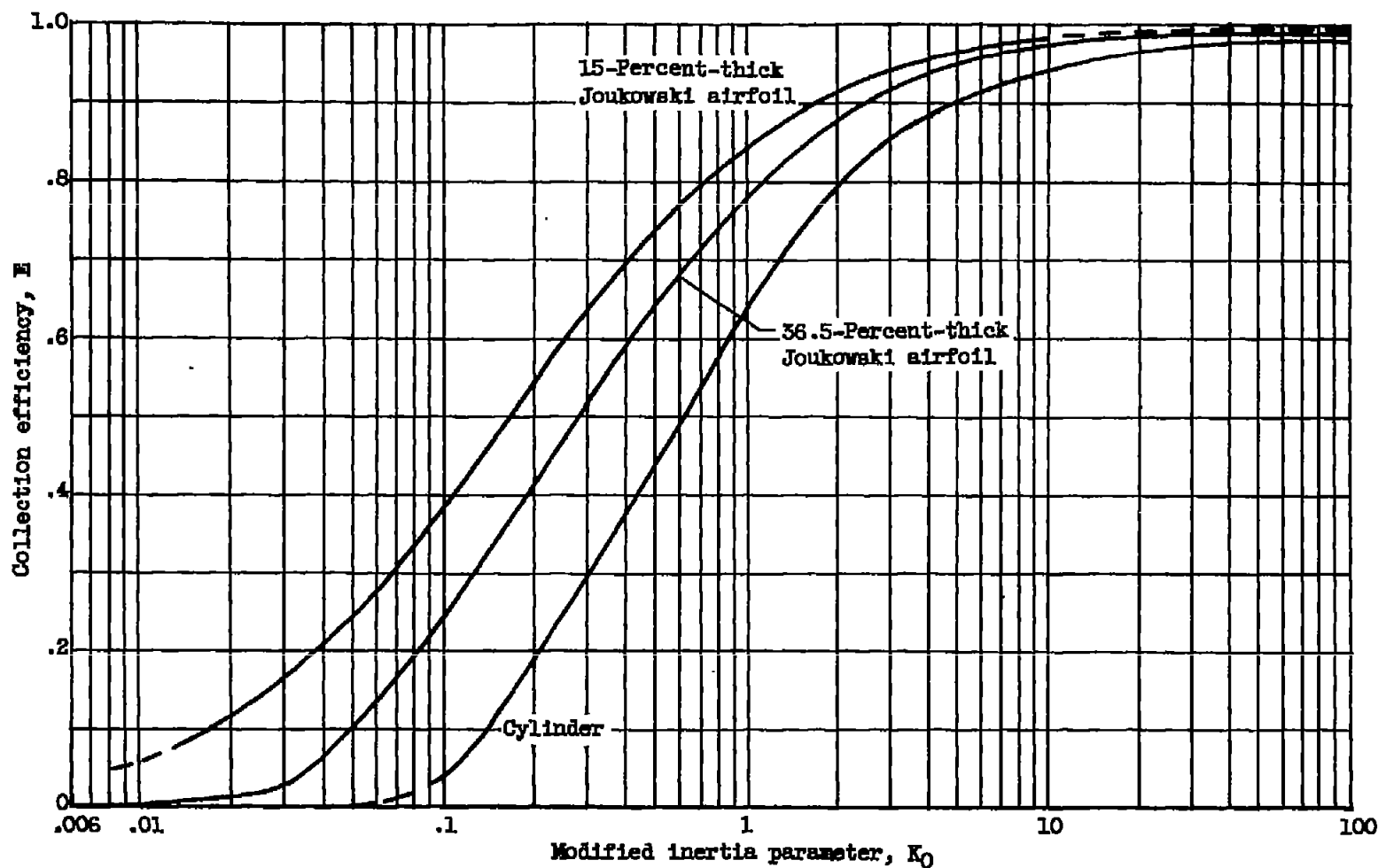
Figure 14. - Comparison of collection efficiency for 15- and 36.5-percent-thick Joukowski airfoils with cylinder.
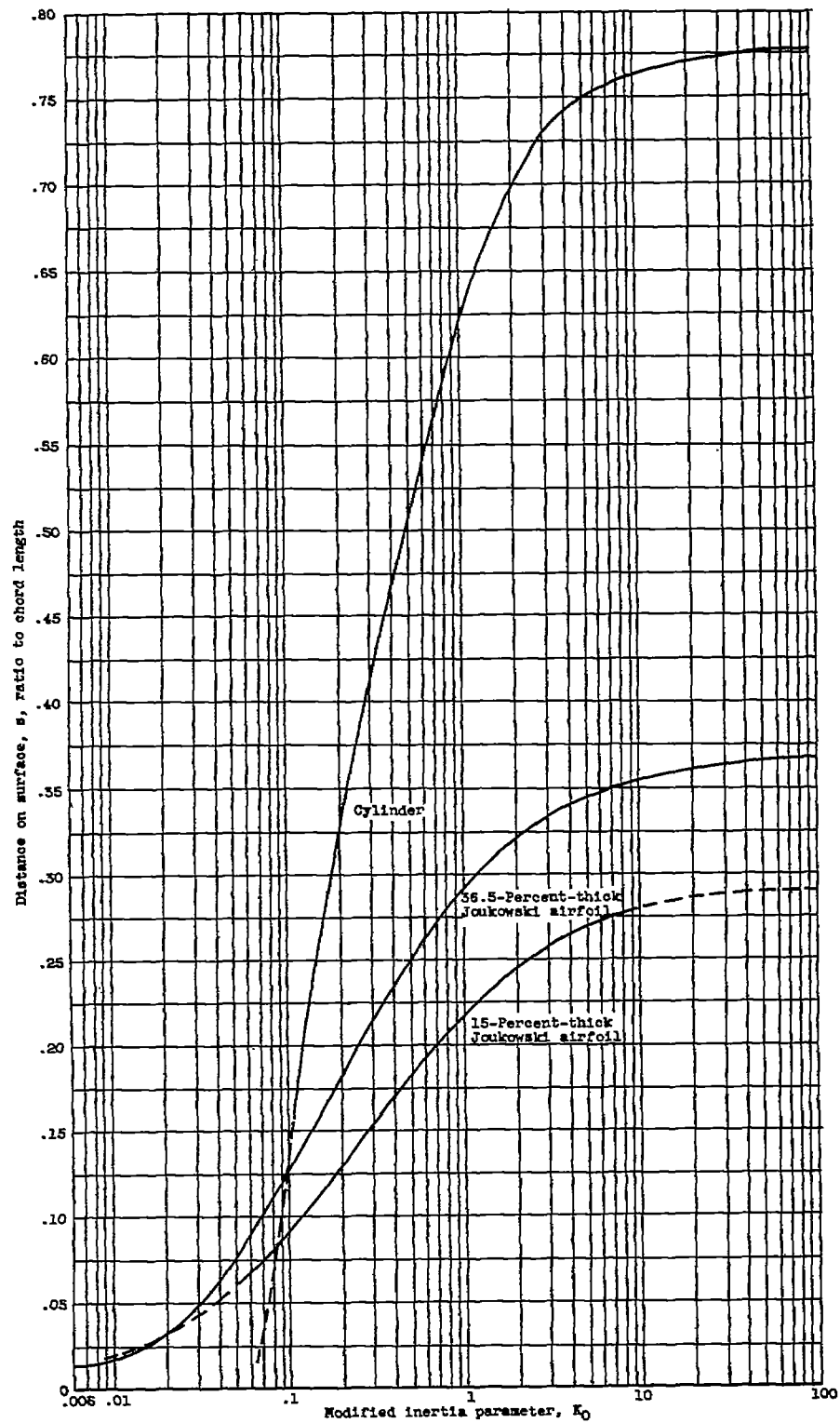
Figure 15. - Comparison of surface extent of impingement for 15- and
36.5-percent-thick Joukowski airfoils with cylinder.
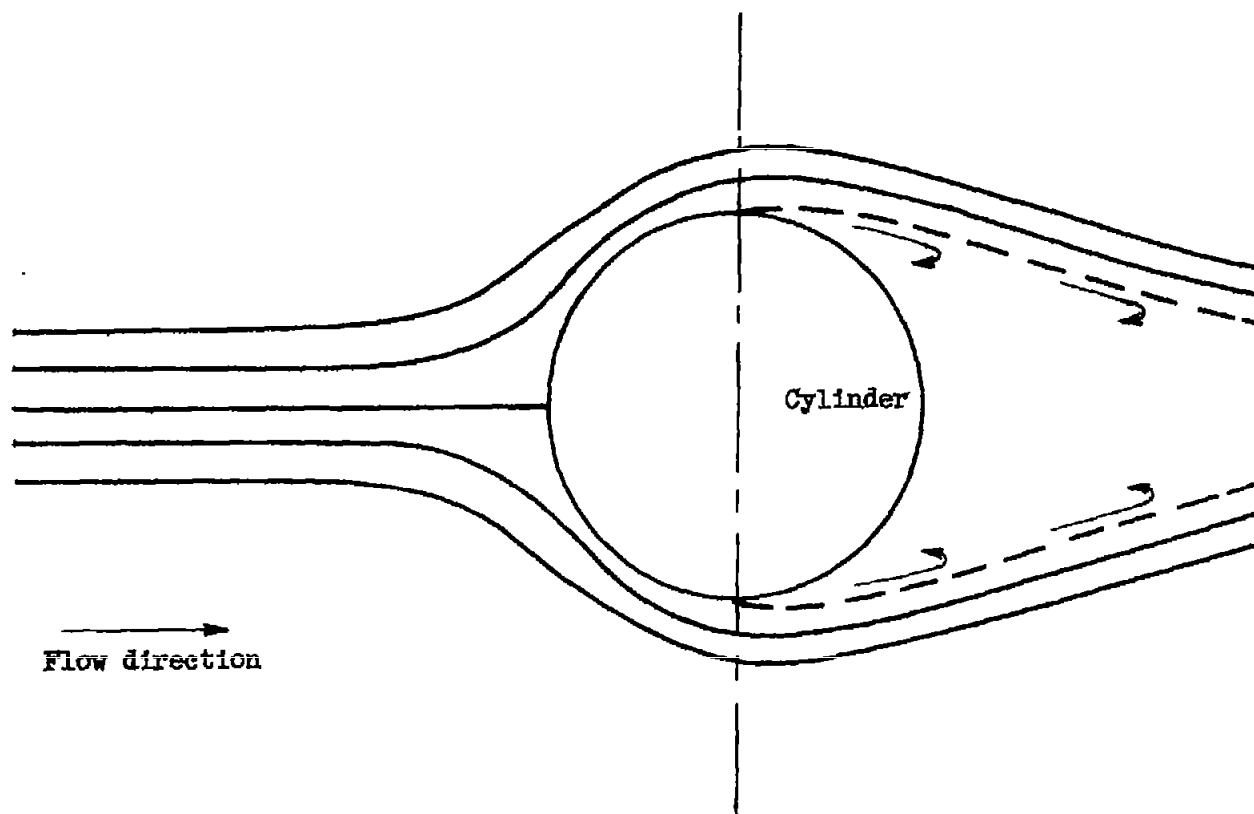
Flow direction

Cylinder

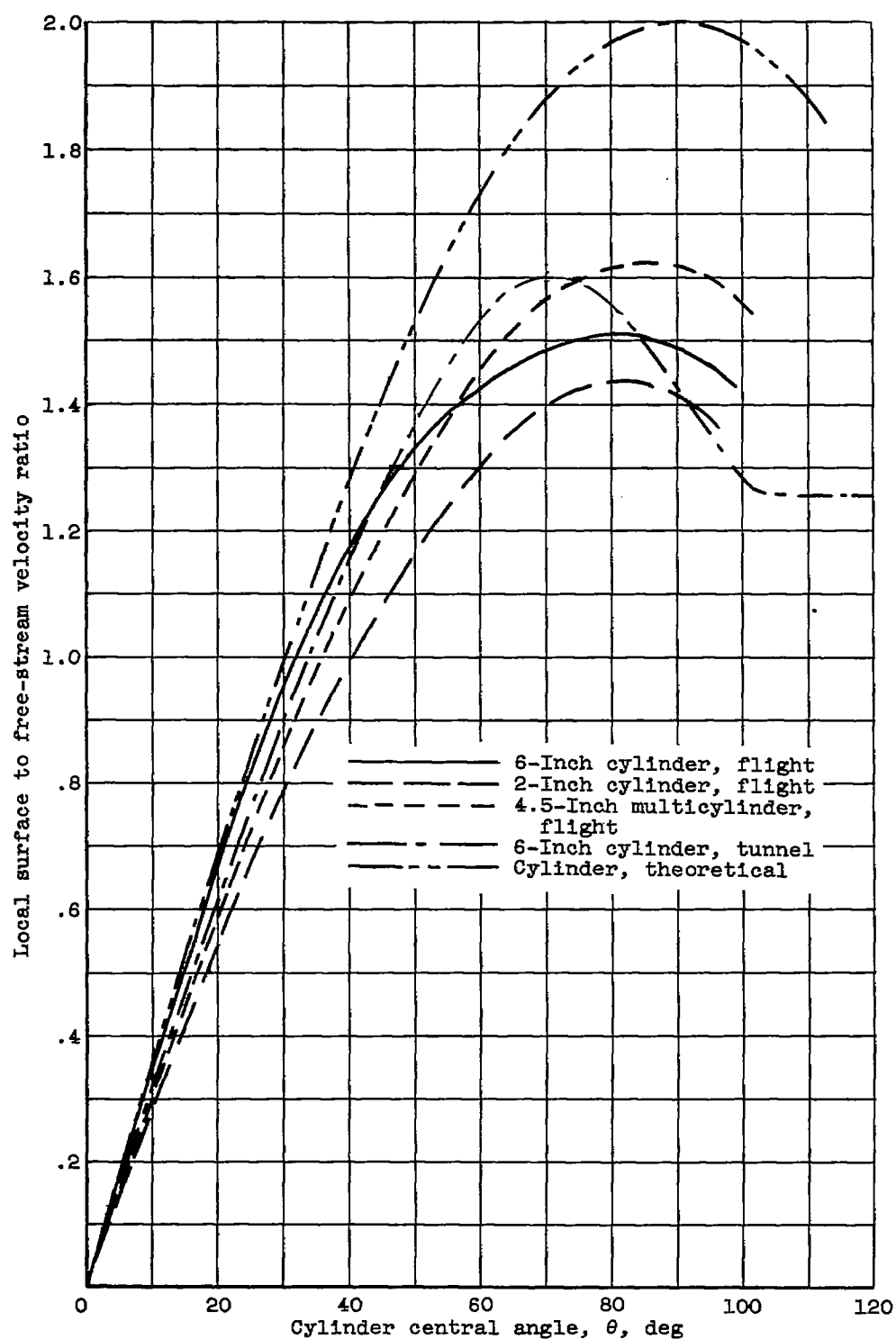Figure 16. - Air streamlines separating from cylinder.

Figure 17. - Comparison of various cylinders in flight and tunnel.
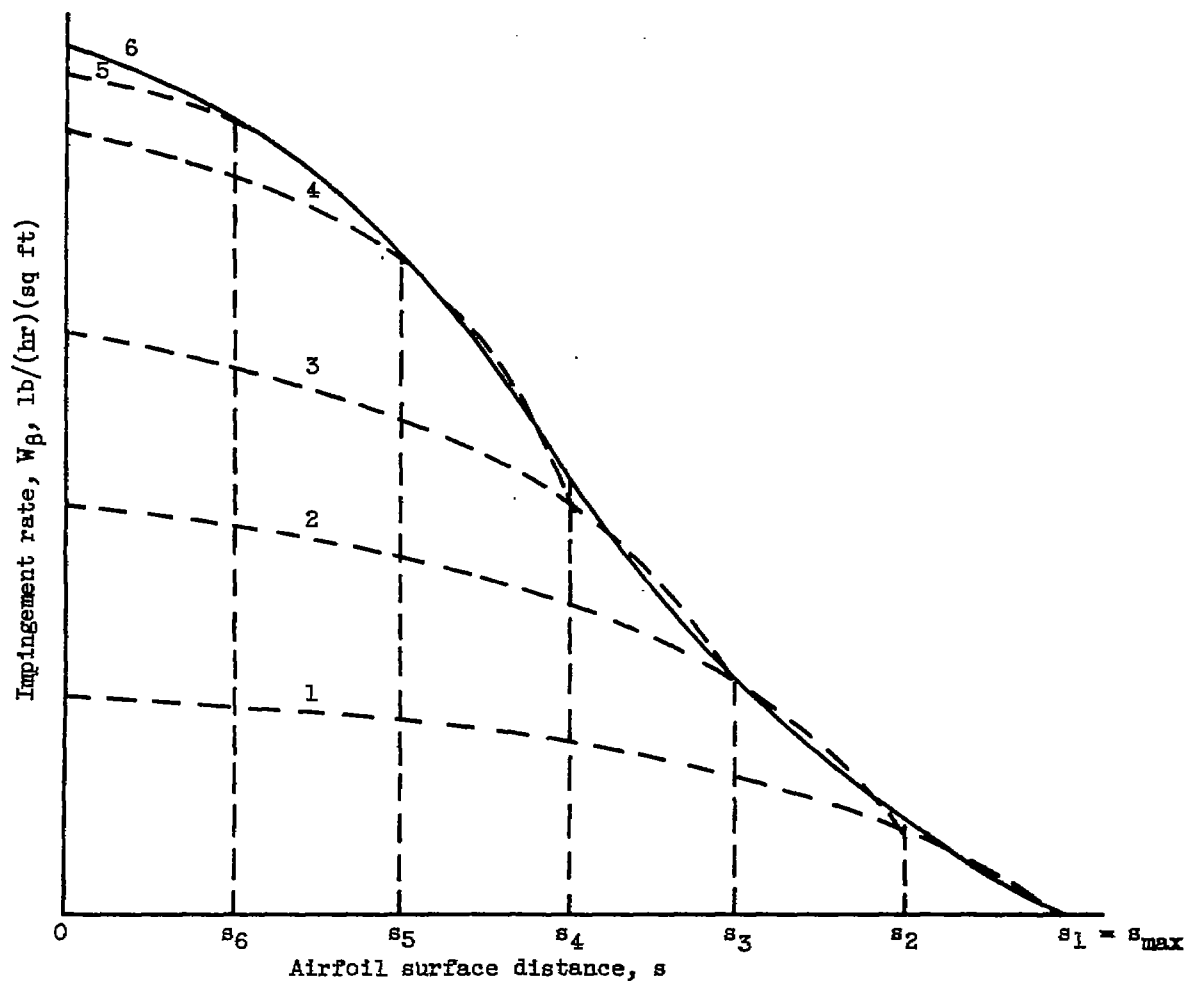Free-stream velocity, 175 miles per hour.

Figure 18. - Illustration of total impingement rate on airfoil surface with contributions from several droplet size groups.